Decoding 3D reach and grasp from hybrid signals in motor and premotor cortices: spikes, multiunit activity, and local field potentials

Arjun K. Bansal, Wilson Truccolo, Carlos E. Vargas-Irwin and John P. Donoghue

J Neurophysiol 107:1337-1355, 2012. First published 7 December 2011; doi:10.1152/jn.00781.2011

J Neurophysiol 107: 1337–1355, 2012.
First published December 7, 2011; doi:10.1152/jn.00781.2011.

Decoding 3D reach and grasp from hybrid signals in motor and premotor cortices: spikes, multiunit activity, and local field potentials

Arjun K. Bansal,[1] Wilson Truccolo,[1,2,3,4] Carlos E. Vargas-Irwin,[1] and John P. Donoghue[1,2,4]
[1]*Department of Neuroscience and* [2]*Brown Institute for Brain Science, Brown University, Providence, Rhode Island;* [3]*Department of Neurology, Massachusetts General Hospital, Boston, Massachusetts; and* [4]*Rehabilitation Research and Development Service, Department of Veterans Affairs Medical Center, Providence, Rhode Island*

Submitted 24 August 2011; accepted in final form 1 December 2011

Bansal AK, Truccolo W, Vargas-Irwin CE, Donoghue JP. Decoding 3D reach and grasp from hybrid signals in motor and premotor cortices: spikes, multiunit activity, and local field potentials. *J Neurophysiol* 107: 1337–1355, 2012. First published December 7, 2011; doi:10.1152/jn.00781.2011.—Neural activity in motor cortex during reach and grasp movements shows modulations in a broad range of signals from single-neuron spiking activity (SA) to various frequency bands in broadband local field potentials (LFPs). In particular, spatiotemporal patterns in multiband LFPs are thought to reflect dendritic integration of local and interareal synaptic inputs, attentional and preparatory processes, and multiunit activity (MUA) related to movement representation in the local motor area. Nevertheless, the relationship between multiband LFPs and SA, and their relationship to movement parameters and their relative value as brain-computer interface (BCI) control signals, remain poorly understood. Also, although this broad range of signals may provide complementary information channels in primary (MI) and ventral premotor (PMv) areas, areal differences in information have not been systematically examined. Here, for the first time, the amount of information in SA and multiband LFPs was compared for MI and PMv by recording from dual 96-multielectrode arrays while monkeys made naturalistic reach and grasp actions. Information was assessed as decoding accuracy for 3D arm end point and grip aperture kinematics based on SA or LFPs in MI and PMv, or combinations of signal types across areas. In contrast with previous studies with ≤16 simultaneous electrodes, here ensembles of >16 units (on average) carried more information than multiband, multichannel LFPs. Furthermore, reach and grasp information added by various LFP frequency bands was not independent from that in SA ensembles but rather typically less than and primarily contained within the latter. Notably, MI and PMv did not show a particular bias toward reach or grasp for this task or for a broad range of signal types. For BCIs, our results indicate that neuronal ensemble spiking is the preferred signal for decoding, while LFPs and combined signals from PMv and MI can add robustness to BCI control.

motor cortex; neural signals; neural coding; brain-machine interfaces; neural prosthesis

ELECTRICAL POTENTIALS recordable extracellularly from the cortex include action potentials ("spikes") and a set of slower field potential events that have been defined mostly by their frequency bands. Spikes and the various subbands of field potentials (FPs) relate to different spatiotemporal scales and are thought to reflect complementary aspects of ongoing sensorimotor processes (Belitski et al. 2010; Mitzdorf 1985; Panzeri et al. 2010). Synaptic currents drive neuronal spiking activity (SA), and their extracellular spatial average is considered a major contributor to FPs (Logothetis 2002). Commonly recognized FP bands in the frontal motor areas include low-frequency local field potentials (*lf*-LFPs or movement event-related potentials, <2 Hz), midrange frequency potentials (~2–30 Hz, including mu and beta bands), and high-frequency LFPs (*hf*-LFPs, ~30–400 Hz). *hf*-LFPs include the gamma band at the low end and mixtures of extracellular action potentials termed multiunit activity (MUA) toward the higher end (Logothetis 2002; Stark and Abeles 2007). Although currently open to interpretation, the *lf*-LFP and *hf*-LFP appear to be related to ongoing sensorimotor processing, while midbands (~2–30 Hz) may be more coupled to attentive or other global processes (Bouyer et al. 1979; Mehring et al. 2003; Rickert et al. 2005) and contain state information (Hwang and Andersen 2009). Understanding the information content and interrelationships of LFP and spiking signals could help reveal the mechanisms of sensorimotor computation. Furthermore, assuming that all of these signals may be amenable to volitional control, this knowledge can be applied to generate useful command signals to drive brain computer interfaces (BCIs) for humans with paralysis (Bradberry et al. 2010; Craggs 1975; Hochberg et al. 2006; Pistohl et al. 2008; Schalk et al. 2007; Waldert et al. 2008, 2009).

Previous studies arrived at inconsistent conclusions when comparing the relative amount of information in SA, MUA, and LFP signals, based on the accuracy with which they can be used to reconstruct reach and grasp kinematics in two (2D) or three (3D) dimensions (Mehring et al. 2003; Stark and Abeles 2007). These studies reached different conclusions about the most informative signal: *lf*-LFP in Mehring et al. (2003) and MUA in Stark and Abeles (2007). This lack of agreement might be due to differences in tasks, areas recorded, decoding algorithms, or number of units/channels considered across these studies. Recent work from our lab focused on low (Bansal et al. 2011)- and very high (Zhuang et al. 2010)-frequency LFPs, without examining the full range of signals or their combinations in hybrid decoders.

To resolve this issue, we directly compared the information content of spikes and selected LFP frequency bands for the same task and decoding methods in a naturalistic 3D reach and grasp task. We also assessed whether information about reach and grasp kinematics in these different types of signals was complementary by comparing performances of decoders that used different combinations of these various signal types. Although optimal input selection approaches using neurons found improved decoding performance (Lebedev et al. 2008;

Address for reprint requests and other correspondence: A. K. Bansal, 3 Blackfan Circle, CLS 13th floor 13077, Boston, MA 02115 (e-mail: arjun.bansal@childrens.harvard.edu).

Santucci et al. 2005; Westwick et al. 2006), the studies comparing SA, MUA, and LFP decoding performance (Mehring et al. 2003; Stark and Abeles 2007) used average-selection approaches. Our analysis was performed with a computationally intensive, greedy-selection-based decoding approach (Bansal et al. 2011; Zhuang et al. 2010) that selected the inputs that contributed the most independent kinematic information. We found that the greedy-selection approach performed better than an average-selection approach taken in previous studies for each class of signal.

Another important issue relates to grasp versus reach processing in ventral premotor (PMv) and primary motor (MI) cortex. Collective results from a number of studies suggest a major role for reach planning and processing in MI and dorsal premotor cortex (PMd; Scherberger et al. 2005; but see Hendrix et al. 2009), grasp processing in PMv (Kurata and Tanji 1986; Prabhu et al. 2009; Rizzolatti et al. 1988), and synthesis of reach and grasp commands within MI networks and through PM-MI interactions. However, recent work has shown that information related to shoulder, elbow, wrist, and digit movement is intermingled in small local neuronal populations and even within individual MI neurons (Vargas-Irwin et al. 2010). Furthermore, neurons related to reach, in addition to grasp, are also present in PMv local ensembles (Bansal et al. 2011; Stark et al. 2007; Xiao et al. 2006). Nevertheless, the relative amount of information about reach and grasp in spiking and the spectrum of LFP signals in premotor and primary motor cortex is unresolved. Here, we directly assessed the information for grasp versus reach in PMv and MI, using a task that uncoupled grasp from reach and was comparable in complexity to those previously used to examine this question. We also assessed the improvements in combining signals across PMv and MI to use any potentially complementary information about grasp and reach across these areas.

To our knowledge, this is the first time such analyses have been performed in the context of a high-dimensional task involving unconstrained reaching and grasping movements using large numbers of electrodes simultaneously recorded in both motor and premotor cortex. The results show that decoding based on small SA ensembles outperforms multiband LFPs in both areas when >16 units (on average) are available, but that *hf*- and *lf*-LFP signals contain significant information about reach and grasp approaching that found in spiking. Surprisingly, despite a prior emphasis on grasp preference in PMv, we found in our naturalistic task no consistent bias between PMv and MI in reconstructing either grasp or reach actions. Overall, our findings suggest that movement information in multiband LFPs is contained within that already available in spiking for neuronal ensembles with >16 units on average, but that combining different types of signals across areas might enhance BCI decoding robustness.

METHODS

All experiments were performed with approval from the Institutional Animal Care and Review Committee (IACUC) at Brown University. The data sets used here have been described in earlier work from our lab (Bansal et al. 2011; Vargas-Irwin et al. 2010; Zhuang et al. 2010).

Continuous Grasping Task

Each of two male macaque monkeys (*monkeys C* and *G*) sat in a chair and was trained to intercept, grasp, and hold various objects, presented one at a time and suspended on a string, that were moving within the arm workspace. Details of this task, briefly summarized here, are provided in Vargas-Irwin et al. (2010). The trajectories and speeds of the presented objects were varied to elicit a wide variety of different reach-to-grasp movements that attempted to uncouple reach location from grasp aperture (see Vargas Irwin et al. 2010 for further rationale). The experimenter's pace in swinging each object over ~2- to 3-s epochs determined the periodicity of the target. The monkeys were rewarded with juice for grasping and holding the suspended object for ~0.5–1 s at any point in the object's trajectory, although the object was swung from an initial location outside the monkeys' reach. Next, they released the object, and then another trial began. The unused hand rested on a contact switch while the task was being performed. Between six and nine objects were used for each of the four sessions, with 20–40 contiguous trials per object. The objects used in the grasping task (Fig. 1 and Supplemental Fig. 1 of Vargas-Irwin et al. 2010) were made of plastic or wood and included balls (2- and 7-cm diameter), cylinders (0.8-cm diameter × 12-cm length and 3.2-cm diameter × 15-cm length), a cube (3.5-cm faces), a rectangular prism (9 × 1.1 × 1.1 cm), an isosceles triangular prism (8.8 × 2.3 × 3.4 cm), a disk (4.2-cm diameter, 1.1-cm thickness), and a ring (7.5-cm diameter, 0.9-cm thickness). Kinematic data were recorded with an infrared optical motion capture system (Vicon Motion Systems, Oxford Metrics Group). This allowed us to obtain a measure of the hand *x*, *y*, *z* position (and correspondingly derive velocity), aperture, and hand speed (norm of the 3D wrist velocity) by tracking reflective markers (4 mm in diameter) placed at various positions along the arm and the hand. The relevant marker positions for this report were one on the wrist (to measure hand position in space) and one each on the distal interphalangeal joints of the index finger and thumb to determine grasp aperture. (Fig. 1*a* in Zhuang et al. 2010). Details of the reconstruction of kinematics from the markers are available in other publications (Artemiadis et al. 2007; Vargas-Irwin et al. 2010). For a detailed analysis of the kinematics of this task and the uncoupling of correlations among arm joint angles and aperture produced by this task, see Vargas-Irwin et al. (2010). For a table showing the mean and standard deviation of the kinematic parameters please refer to Table 1 of Zhuang et al. (2010). Overall, reaches covered most of the workspace, with grasps occurring across a varied distribution of workspace locations.

Neural Data Recording and Preprocessing

Neural recording was performed in two monkeys with two chronically implanted microelectrode arrays [Blackrock Microsystems, Salt Lake City, UT; 4.2 × 4.4 mm; 96, Si electrodes (1-mm length) coated with Parylene] in four sessions (2 sessions for each monkey). Array types and details of surgery are similar to those described previously (Suner et al. 2005), except that two arrays were implanted in each monkey. Arrays were implanted in arm/hand regions of MI and PMv (contralateral to hand used for task) in both monkeys. The MI implantation site was rostral to the central sulcus at the level of the genu of the arcuate sulcus, where neurons related to arm movements have been widely recorded (Lemon 1993). The PMv implantation site was just caudal to the arcuate sulcus at the level of the principal sulcus, where hand grasp signals have been identified (Kurata and Tanji 1986; Rizzolatti et al. 1988) corresponding to the F4/F5 boundary.

Data acquisition and storage were accomplished with two (1 for MI, 1 for PMv) Cerebus multichannel data acquisition systems (Blackrock Microsystems). The amplifier sampled voltage data at 30 kHz from each channel. LFP data were collected by band-pass filtering the sampled voltage traces between 0.3 and 500 Hz and

storing them at 2-kHz sampling rate. All 96 LFP channels were stored for *monkey G*, while 48 LFP channels were stored for *monkey C* because of technical constraints at the time of recordings. Spiking activity was collected by first band-pass filtering the amplifier output between 0.3 Hz and 7.5 kHz and then thresholding the resulting signal at 4.5 times the standard deviation of the amplitude of recordings during an initial baseline period of ~1 min. This was followed by extracting a 1.6-ms, 48-sample waveform for each spike. Spiking activity was collected from all 96 channels in each array in both monkeys. Collected spiking activity comprised of both single and multiple units. An automatic spike sorter (Vargas-Irwin and Donoghue 2007), along with manual oversight and correction, were used to identify putative single units that were extracted from the thresholded filtered signal. A signal-to-noise ratio (SNR; see Vargas-Irwin and Donoghue 2007 for definition) threshold of 1.5 was used for *monkey G*, *session 2*, to extract well-isolated single units. The data from *monkey G*, *session 1*, and *monkey C*, *sessions 1* and *2*, also included, besides well-isolated units, putative units that might have contained spikes from more than one neuron (SNR $<$ 1.5). The number of spiking units in each session from MI and PMv are listed in Table 1.

Recording sessions lasted ~1 h. The sessions were 8 days apart in *monkey G* and 3 mo apart in *monkey C*, with the first sessions 12 days and 30 days after array implant in each monkey, respectively. All recorded LFP channels were considered for building decoders (see next section).

Data analysis was performed with custom software written in MATLAB (MathWorks, Natick, MA).

Decoding

Information was assessed by decoding performance rather than information theoretic measures such as mutual information, because reasonable estimates of these quantities require larger sample sizes not feasible in these experimental sessions.

The power spectrum of the kinematics variables (position, velocity, and aperture) was dominated by peaks in low-frequency components ($<$2 Hz) in our task. Kinematic data were consequently filtered with a Kaiser filter (Belitski et al. 2008; Kaiser 1974) with a 2-Hz cutoff. LFP data were filtered by using different Kaiser filters for the different bands [LF: low pass with 2-Hz cutoff; *hf*-LFP band 1 (H1): 100–200 Hz band-pass filter; *hf*-LFP band 2 (H2): 200–400 Hz band-pass filter] and then downsampled from 2 kHz to 1 kHz. These particular LFP frequency bands were selected because single-channel mutual information analysis in previous work demonstrated that these bands contained most information about kinematics (Zhuang et al. 2010), similar to results in primary visual cortex related to stimulus information (Belitski et al. 2008). In particular, previous analysis (Zhuang et al. 2010) of the same data has shown that the higher-frequency bands ($>$100 Hz) yielded better decoding performance for these areas and tasks than the typically defined gamma band (~30–100 Hz). The LFPs were filtered with zero-phase filtering (filtfilt in MATLAB) to avoid phase distortions at different frequencies. The results presented here are based on decoding performed at 50-ms time steps (20 Hz). We averaged the kinematic signals (x, y, z position, x, y, z velocity, aperture, or hand speed) within 50-ms windows. Kinematics were paired with collected and averaged neural activity (SA and LFPs) in an immediately preceding 150-ms time window. These time windows and time-step updates were selected after initial explorations (see also Zhuang et al. 2010 for more details). In addition, for the H1 and H2 bands, amplitudes were squared before averaging over the time window, whereas no squaring was performed for the LF band. All neural signals were normalized by mean subtraction and dividing by the standard deviation prior to their use in the Kalman filter.

Table 1. *Total number of units recorded in two sessions in monkeys C and G*

	MI	PMv
Monkey C, *session 1*, 12/12/07	136	99
Monkey C, *session 2*, 3/19/08	115	142
Monkey G, *session 1*, 7/2/08	76	171
Monkey G, *session 2*, 7/10/08	30	108

Monkeys were implanted on 11/30/2007 and 6/2/2008, respectively. MI, primary motor cortex; PMv, ventral premotor cortex.

Kalman filter for decoding. Similar to methods of Zhuang et al. (2010) and Bansal et al. (2011), a linear Gaussian state-space representation and the corresponding Kalman filter were used to decode reach and grasp kinematics from the LFP and from spike counts. The state-space model was given by

$$x_k = Ax_{k-1} + \varepsilon_k$$

$$P_{i,k} = Hx_k + \eta_k$$

here x_k is a given (zero mean) kinematic variable, k indexes time, and $P_{i,k}$ corresponds to the LF amplitude, H1 or H2 squared amplitude, or spike counts depending on the type of input as measured on the ith electrode (or the ith unit). A and H are the state and observation matrices, respectively, and $\epsilon_k \sim \mathbf{N}(0, Q)$ and $\eta_k \sim \mathbf{N}(0, R)$, are the state and observation Gaussian noise, respectively. Parameters in state-space and the Kalman filter solutions were estimated and computed with an algorithm described previously (Wu et al. 2006).

The decoding was cross-validated by using the data from $n - 1$ objects within a session for training and testing on the trials that were not used for training ("leave-one-object-out" cross-validation). Besides addressing the overfitting issue, this cross-validation scheme also evaluated how well the Kalman filter models generalized across different objects.

Performance of n-Best Units/Channels

Greedy-selection procedure. To examine the performance obtained by progressively adding LFP channels (or spiking units) to the pool used for decoding using Kalman filter, we first selected the best channel (or unit) among the total number of channels (or units) based on decoding accuracy (Pearson correlation coefficient r, between measured and reconstructed kinematics). At each subsequent step the channel (or unit) that contributed the most independent information was added to the existing pool of channels (or units). For example, we then selected the best 2 channels (or units) including the already selected channel (or unit), i.e., we added the channel that improved reconstruction the most over the already selected channel. Next we selected the best 3 channels (or units) including the already selected best 2 channels (or units), and so on, up to a maximum of 50 inputs (or the maximum number of channels or units, if these were lower). We restricted the maximum numbers of inputs to 50 in the greedy search of optimal subsets because of constraints in the amount of computational time, but this also serves to balance the numbers of inputs across spiking units and LFP channels (typically, there were more spiking units than LFP channels). We refer to this method of selecting inputs as the "greedy" procedure in this article. In the end, the optimal subset of inputs corresponding to the one that yielded the maximum r was selected as the output of the greedy-selection procedure. Previous results (Vargas-Irwin et al. 2010) and our preliminary analysis suggested that the decoding performance saturates after the addition of ~30 (best) input channels.

To address the possibility that one type of signal (e.g., spikes vs. LFPs) may overfit the training data more than other signal types, and therefore be selected more often as optimal inputs in hybrid signal decoders (see below), we also adopted a variation of the above greedy decoding approach (see Figs. 9 and 10). In this case, the reported fraction of selected signal types in hybrid decoders was obtained from a cross-validation scheme in which the parameter estimation for the Kalman filters and the selection of optimal inputs for hybrid decoders

were based on different data segments. We divided the data for each object into three segments consisting of 50%, 25%, and 25% of the time recorded for reaching/grasping each object. Each of these segments was concatenated across objects for each session in each monkey to form the training data for the Kalman filter parameters, the training data for input selection, and the cross-validation test data for reporting decoding performance, respectively.

The three-step procedure was as follows:

In *step 1*, we used the training data for the Kalman filter from all n objects to build the Kalman filter.

In *step 2*, we iteratively added the inputs (by using the corresponding submatrix of the Kalman filter weights) that increased the performance of the Kalman filter (built in *step 1*) the most at each number of inputs, using the training data for input selection.

In *step 3*, we computed the decoding performance on the optimal subset of inputs selected in *step 2* on the cross-validation test data.

Statistical significance of observed r. Previous studies from our lab analyzing the same data used a random permutation test (phase-randomization; Bansal et al. 2011; Zhuang et al. 2010) and found that typically r values above 0.2 were significantly better than "chance" level decoding. That is, r values above 0.2 fell above the 99.9% confidence bound of reconstruction, which could be achieved by using a phase-randomized version of the LFP signal.

Normalized root mean squared error. Decoding performance was also evaluated by using a normalized root mean squared error (nRMSE) measure for each kinematic parameter. This was defined as

$$\text{nRMSE} = \left[\text{Mean}\left[\left(x_k^{\text{reconstructed}} - x_k^{\text{observed}}\right)^2\right]\right]^{1/2} / \left[95\%\text{ range of } x_k^{\text{observed}}\right]$$

For each time step k that was within the 95% range of the observed, measured kinematics, $x_k^{\text{reconstructed}}$ were the reconstructed kinematics using the Kalman filter and x_k^{observed} were the corresponding observed kinematics.

Average case. For the average-case analysis (see Fig. 5) we picked n input channels (or units) at random instead of picking the best n channels (or units), for 100 draws at each input number. The average was defined as the mean of this population and is designed to show how any typical population sampled using this array might perform.

Multiarea, Multiband LFP, or Hybrid Signal Decoding

Decoding independent of the area or of the signal type was performed to determine which combination of areas or signals provides the best signal reconstruction. We termed these multiarea (MA), multiband LFP (*mb*-LFP), or hybrid signal (HS) decoding. For MA decoding we pooled signals of the same type (LF, H1, H2, or spikes) across both MI and PMv and performed the same greedy selection of optimal subsets (up to a maximum of 50 input channels or units) followed by Kalman filter decoding as described above. For multiband LFP signal-based decoding (*mb*-LFP) we pooled LFP signals (LF, H1, and H2 bands) from both MI and PMv and performed a similar greedy selection as for MA, so that the decoder could select from any combination of LFP signals. Finally, we created a decoder based upon signals of all types sampled from both areas, termed HS decoding.

RESULTS

Simultaneous broadband LFP (0.3–500 Hz) and spike recordings in MI and PMv were obtained from two monkeys in two sessions each while they performed a continuous reach and grasp task (see METHODS). Following previous studies (Bansal et al. 2011; Belitski et al. 2008; Rickert et al. 2005; Stark and Abeles 2007; Zhuang et al. 2010), we compared decoding performance of eight different reach and grasp parameters (3D hand position, 3D velocity, finger-thumb aperture, and hand speed), using low and high LFP bands and spiking activity (Fig. 1).

The overall organization of this section is as follows. The first part focuses on the relative comparison of information in the different signal types, while the second part combines different signal types together and examines the corresponding improvement in reconstruction performance. For each part, we also examine the areal differences in relative information about grasp versus reach, using signals from PMv versus MI. We finish with two sections that test even more rigorously the strength of our main results. Detailed results of our analyses and statistical tests are presented in Tables 2–6.

Spikes Generally Outperform LF, H1, and H2 LFP Bands in Decoding 3D Reach and Grasp

We examined whether spikes or LFPs contained different amounts of information about reach and grasp in PMv and MI. We evaluated the information content of SA and three LFP bands (LF: 0.3–2 Hz; H1: 100–200 Hz; H2: 200–400 Hz) based on their ability to predict continuous kinematic parameters during reaching and grasping. We then compared the accuracy of decoding using the greedy-algorithm-selected subset of units or channels for each band (Figs. 1–5). Decoding was performed with Kalman filters and n-fold cross-validation for each data set, where n was the number of objects used in that session (see *Decoding*, METHODS).

Figure 2, *A–K*, give typical examples of decoding two kinematic parameters (z-position and aperture) using four different signals in MI, for one session in *monkey C* extending ~20 s (for ease of visualization). We present z-position and aperture for illustration, but the decoding performance for all other kinematic parameters was similar. (The complete set of decoding results for all parameters is presented in Fig. 4.) Inspection of reconstructions shows qualitatively that all signal reconstructions follow the general shape of each of the parameters tested, but spikes captured the details of kinematics better than the LFP bands, as can be appreciated in Fig. 2.

Most commonly, spiking provided the best decoding, with the relative performance of LFP bands depending on the decoded kinematic parameter. The fit between decoded signal and kinematics is quantitatively presented in Fig. 3, *A–D*, which show the Pearson's correlation coefficient (r) between original and reconstructed kinematics for increasing numbers of input channels or units. For each session, the greedy-selection procedure found the "optimal" subset of up to 50 inputs that gave the maximum r (indicated by triangular markers in Fig. 3, *A–D*) for each type of signal. In 23 of 64 (36%) instances (64 instances = 8 kinematic parameters × 2 monkeys × 2 areas × 2 sessions each), the relationship in the decoding performance was SA > H2 > H1 > LF (see Fig. 3, *A–C*, for examples). However, the order for LFP bands was commonly reversed so that lower frequencies were next best after spiking. SA > LF > H2 > H1 was seen in 18 of 64 (28%) instances. More generally, we observed a trend of SA giving better r than H2, H1, and LF bands when pooling information across multiple electrodes (53/64 or 83% of instances). In 11 of 64 (17%) instances, however, one LFP band gave better r than SA-based decoding. For example, in Fig. 3*D*, LF performed better than spiking and H1 and H2 bands. When considered on a single-channel basis LFPs were typically better: The median

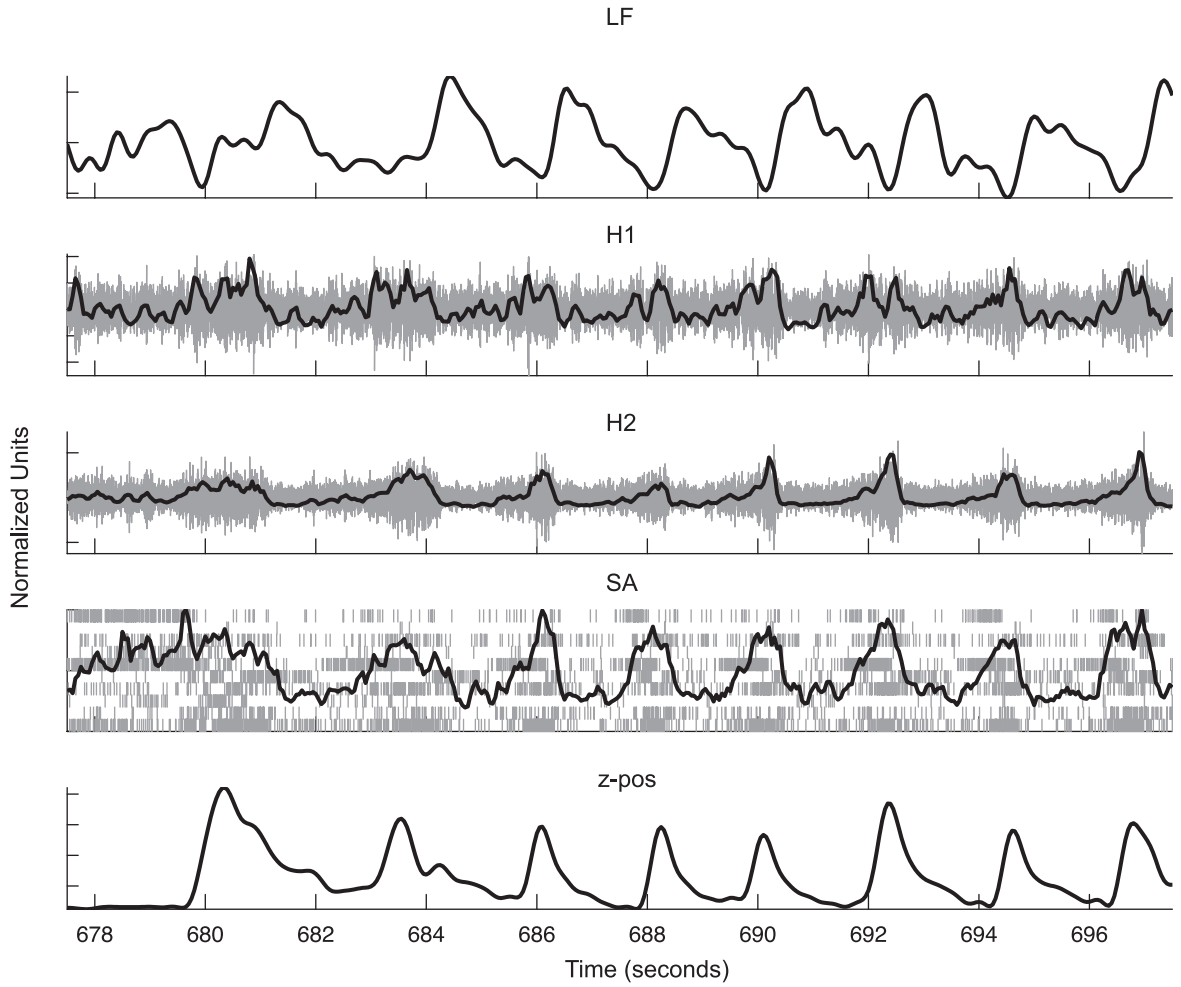

Fig. 1. Examples of the 4 different neural signals used for decoding in this study: low-frequency local field potentials (LFPs) (LF, 0.3–2 Hz), high-frequency local field potentials (H1 band, 100–200 Hz; H2 band, 200–400 Hz), and spiking activity (SA) during the same time period from *monkey C*, *session 2*, primary motor cortex (MI). For each of the LFP signals, the channel that gave the single best performance was selected and plotted. For the H1 and H2 signal the filtered signal is shown in gray, and the signal squared and averaged in 150-ms windows (as used for decoding) is shown in black (see METHODS). For the spiking signals, the rasters for the top 10 performing units are plotted (gray vertical lines) along with the averaged spike counts across those 10 units (solid black line). *Bottom*: measured value of 1 of the 8 kinematic parameters (z-position) that were decoded in this study, during the corresponding time period.

r values for LFP channels considered separately were larger than SA in 73% of cases (illustrated for a few cases in *insets* of Fig. 3, *A*, *B*, and *D*; the median was computed across all input channels or units used for building the corresponding greedy decoder).

Figure 4 summarizes the ensemble (a group of LFP channels or units) decoding results presented by showing the performance of the optimal subset of channels or units selected with the greedy method for each kinematic parameter (as shown in Fig. 3, where the results using the optimal subset are indicated by inverted triangle markers). Overall, the majority of instances (244/256; 256 = 4 signal types × 8 kinematic parameters × 2 monkeys × 2 areas × 2 sessions), including all instances of H2-based and spike-based decoding, gave above-chance decoding performance for all kinematic variables (Fig. 4, *A* and *B*). On average (across monkeys, sessions, areas, and kinematic parameters), spike ensembles gave higher r than any of the LFP bands (see Table 2.1: notation means Table 2, *column 1*).

Spike-based decoding was significantly better than any of the LFP bands both in MI and PMv. However, these average results did not mean that spiking ensembles always were better at decoding than LFP in every instance. As mentioned above, LFP ensembles performed better (greater r) than spiking ensembles in 11 of 64 instances (17%). Despite this observation, the average (across monkeys and sessions) decoding performance for any kinematic parameter using LFPs was never statistically better than that obtained using spikes. At its best, on average LF gave statistically no different performance compared with spiking in decoding z-velocity in PMv (mean r: LF 0.73 vs. spikes 0.72; $P = 0.88$). Thus on average spikes gave better r than LFPs in both MI and PMv.

Decoding performance for different LFP frequency bands varied according to the kinematic parameter decoded, but certain trends were evident. The overall trend was that the higher frequencies outperformed the lower frequencies. Specifically, H2 decoding was never significantly exceeded by other LFP bands (Table 2.2, 2.3). For velocity decoding, H2 was not significantly different from LF, and LF outperformed the H1 band ($P < 0.01$, Table 2.2). In addition, we did not find any consistent superiority in decoding using signals from MI or PMv by signal type (Fig. 4*E*) or kinematic parameter (Fig. 4*F*).

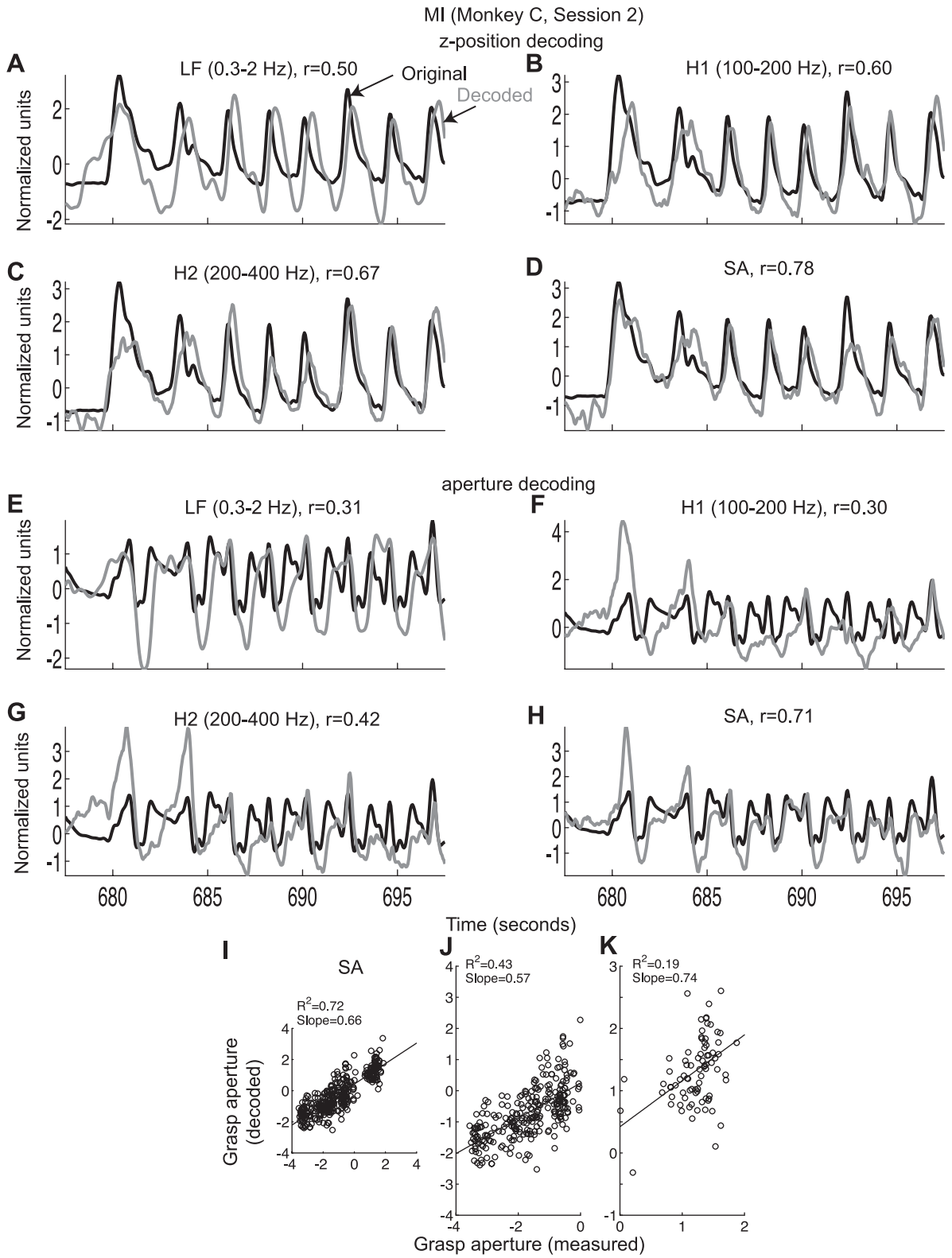

Fig. 2. Examples of decoding kinematic parameters using each of the 4 neural signal types separately from multiple electrodes in MI. Decoding of *z*-position (*A–D*) or aperture (*E–K*), in *monkey C*, *session 2*, using the best combinations of inputs (as ascertained with the greedy algorithm, see METHODS) for each of the 4 neural signals from MI, for the same time segment shown in Fig. 1. *A* and *E*: LF (0.3–2 Hz). *B* and *F*: H1 band (100–200 Hz). *C* and *G*: H2 band (200–400 Hz). *D* and *H*: spiking activity (SA). Original kinematics in black, decoded in gray. *r* values were computed on the entire reconstruction for each parameter and not just for the time segment displayed here. *I*: normalized aperture amplitude at grasp completion (i.e., at the time the object is actually grasped; 1 sample per trial) tended to cluster in 2 groups corresponding to objects that required either a decrease or an increase in aperture relative to the mean aperture during the session. Decoders captured variations in this aperture amplitude across the 2 clusters, as shown for the example of SA-based decoder in *I*. *J* and *K*: in some cases, it was also possible to capture trial-by-trial variations in aperture amplitude within the same cluster. The slope for the best-fit line and corresponding coefficient of determination R^2 for the fit are shown ($P < 10^{-3}$).

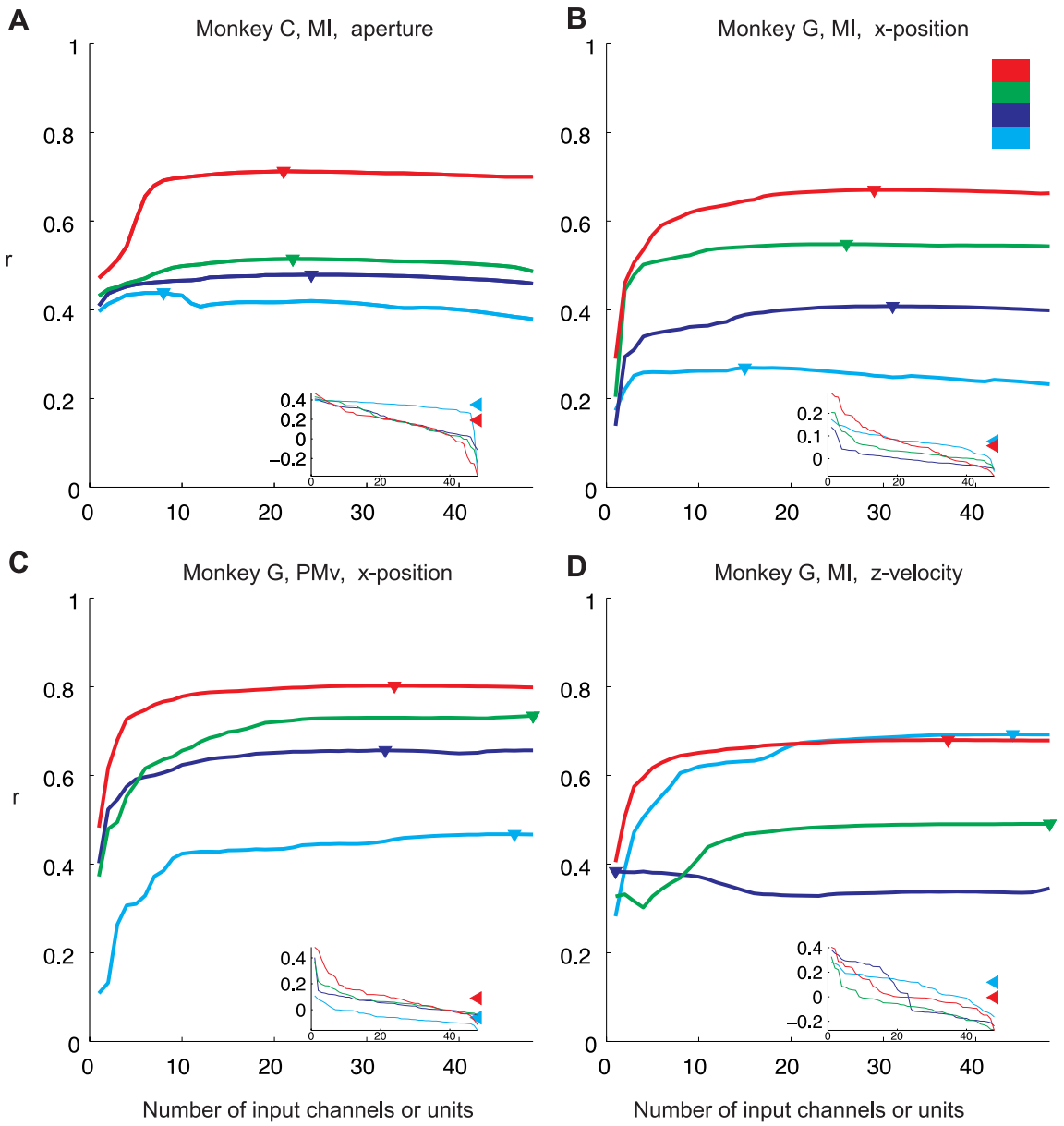

Fig. 3. Examples of greedy-selection-based decoding. This figure illustrates the impact of increasing the numbers used of each neural signal type's inputs on kinematic decoding performance. Results of greedy-selection decoding for each of the 4 different signals and for decoding aperture in *monkey C*, MI (*A*), *x*-position in *monkey G*, MI (*B*) or ventral premotor cortex (PMv) (*C*), and *z*-velocity in *monkey G*, MI (*D*) (from *session 1* for each monkey) are shown. Four signals were compared: LF, H1, H2, and spiking units. Inverted triangular markers indicate the optimal subset of inputs and the corresponding maximal *r* for each signal. *Insets* plot the correlation coefficient (*r*) when decoding from each of the top 48 (corresponding to those selected by the greedy algorithm) individual units or channels separately in rank order determined by single-channel performance. The medians of the single unit or LF channel performances are indicated with corresponding left-pointing triangles. Note that *r* for some of the LFP channels or SA units, when used 1 channel or 1 unit at a time respectively, could sometimes be negative. Individual LFP channels or units that did not contain significant kinematic information sometimes gave negative *r* values on cross-validated data. However, when decoding using multiple input channels or units, at the final step of the greedy algorithm we selected the best subset of LFP channels or SA units, thereby eliminating the deleterious effect of these individual negative *r* inputs.

Mean squared error. Using nRMSE (see METHODS) as another measure of decoding performance revealed the same trend as for *r*. The *r* between original and reconstructed kinematics can be high but contain signal reconstruction errors, as for example when there is a constant offset between two signals. Therefore, to gain an additional measure of the quality of reconstruction using each of the different signals, we also determined the least nRMSE between original and reconstructed kinematics (Fig. 4, *C* and *D*) as a second measure of decoding performance that captures bias in the reconstructions. We found that the nRMSE was on average greatest (i.e., poorest reconstruction) for LF, followed by H1 and H2 bands, and the least for spikes (Table 2.4), consistent with the results found from the *r* measure. Spikes yielded the least nRMSE in 45 of 64 or 70% of cases (i.e., performed best). The order effect from high to low error (LF > H1 or H2 > SA) was present in 22 of 64 (34%) individual cases, while H1 > LF > H2 > SA was found in 13 of 64 (20%) cases. Thus these analyses supported the generally better decoding of spiking as found using *r*. We also found that the relative ranking of different

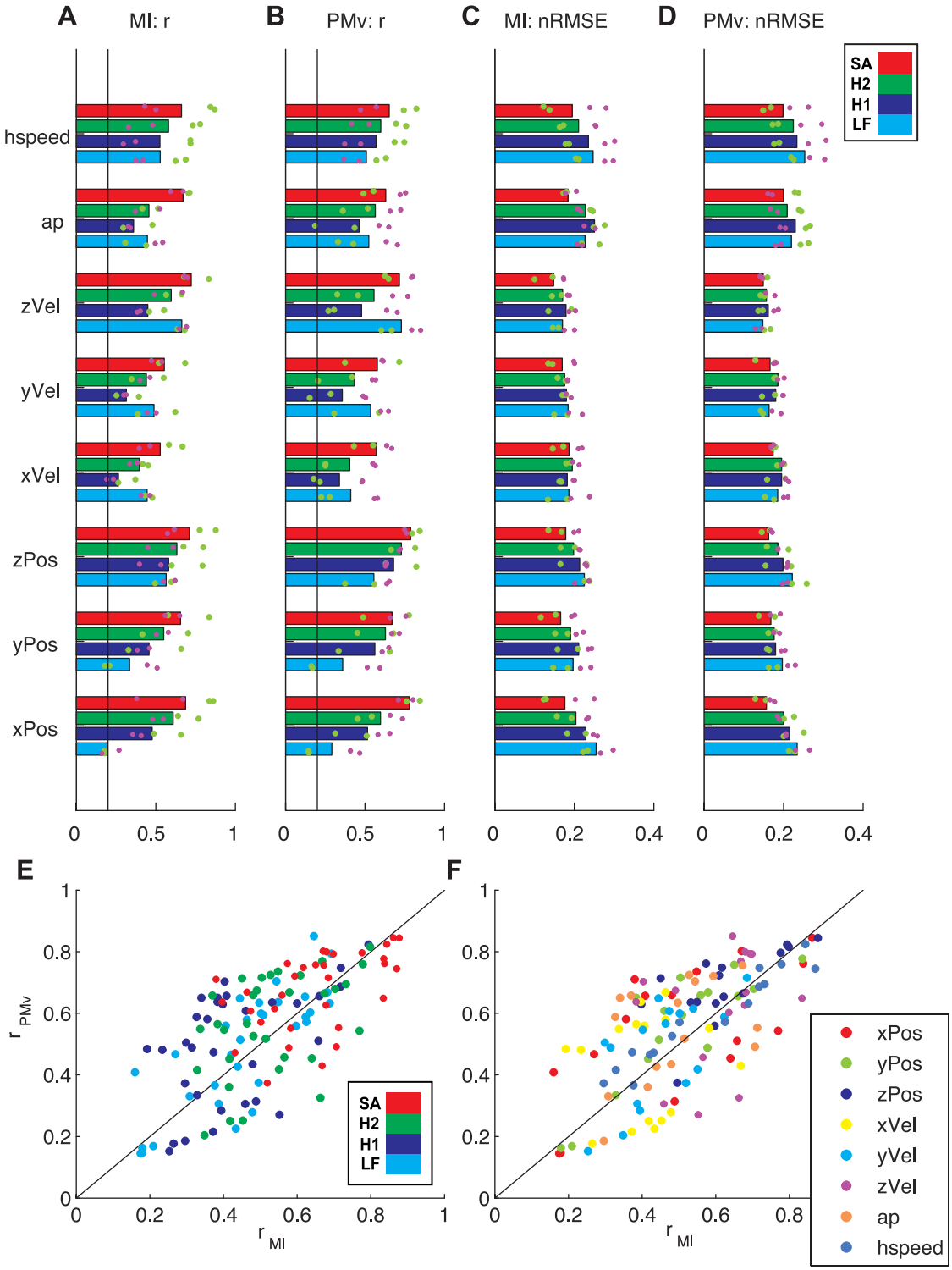

Fig. 4. Summary of optimal kinematic decoding performance with each neural signal. Optimal subsets of input channels corresponding to those yielding the maximum correlation coefficient between original and reconstructed kinematics were selected for each signal with a greedy-selection procedure (see METHODS). Results are the individual kinematic parameter decoding data maximum correlation coefficients (r) (*A*, *B*) or the corresponding least normalized root mean squared errors (nRMSEs) (*C*, *D*) for the entire data set [8 kinematic parameters decoded with data from 2 sessions in each of 2 monkeys (*monkey C*, light green; *monkey G*, magenta) in MI (*A*, *C*), and PMv (*B*, *D*)]. In *A–D*, bars indicate the mean of the max r or mean nRMSE between original and decoded kinematics (color convention similar to Fig. 3) and dot markers represent individual session results. Vertical line at $r = 0.2$ indicates the significance threshold (see METHODS). Based on the random permutation test (see METHODS), all r averages (by kinematic parameter for each signal) were above chance except LF decoding of x-position using MI data (average = 0.196). We also plot the r for MI vs. PMv comparing decoding performance in the same session, by signal type (*E*) or by kinematic parameter (*F*). Note that decoding performance for both grasp aperture and reach parameters was comparable across PMv and MI.

Table 2. *Results for spike and LFP decoding*

Signal/Comparison	1. Mean *r* (all parameters)	2. Mean *r* (*x*, *y*, *z* velocity)	3. Mean *r* (position parameters)	4. Mean nRMSE (all parameters)
Statistical test or note	Mean sig. diff. (all pairs)	Mean sig. diff. (all pairs)	Mean sig. diff. (all pairs)	Mean sig. diff. (all pairs)
LF	0.47 ± 0.02 (†H1, H2) (*SA)	0.55 ± 0.03 (*H1) (†H2, SA)	0.38 ± 0.04 (*H1, H2, SA)	0.21 ± 0.04 (†H1, H2) (*SA)
H1	0.46 ± 0.02 (‡H2) (*SA)	0.37 ± 0.03 (†H2) (*SA)	0.55 ± 0.03 (†H2) (*SA)	0.20 ± 0.04 (†H2) (*SA)
H2	0.55 ± 0.02 (*SA)	0.47 ± 0.03 (*SA)	0.62 ± 0.02 (†SA)	0.19 ± 0.03 (‡SA)
Spikes	0.66 ± 0.02	0.61 ± 0.03	0.71 ± 0.03	0.17 ± 0.04
All signals	0.53 ± 0.01	0.50 ± 0.02	0.57 ± 0.02	0.19 ± 0.04

Values are means ± SE unless otherwise noted. LF, low-frequency local field potential (LFP) band; H1, H2, high-frequency LFP bands; SA, spiking activity; *r*, correlation coefficient; nRMSE, normalized root mean squared error. ANOVA with Dunn-Sidek correction for multiple comparisons was used, unless indicated otherwise: *$P < 0.01$, ‡$P < 0.05$, †not significant ($P > 0.05$). For example, *SA represents that the mean was found to be significantly different from the mean performance for spikes at the $P < 0.01$ level. Significance relationships were symmetrical and hence are not listed repeatedly for both compared signals.

signals was not specific to the quantity optimized (Pearson's correlation coefficient) in the greedy subset selection but was also maintained when the nRMSE was minimized instead.

Greedy selection outperforms average selection. The above results could be attributed to the way the greedy-algorithm-selected inputs for the decoder compared with an average-selection approach used in previous studies (Mehring et al. 2003; Stark and Abeles 2007). Our preliminary analysis (Bansal et al. 2011) had suggested that the greedy selection might perform better than average selection, and could influence the relative ranking of low-frequency LFPs and spiking signals even for decoding the same kinematic parameter. However, because of earlier computational resource constraints, we were limited to analyzing only 4 of 256 instances (1 kinematic parameter for 1 area in each monkey for 1 session, using LF or SA). To comprehensively determine how greedy versus average selection influences the relative ranking of signal types in decoding 3D reach and grasp kinematics, we performed the same analysis as in Figs. 3 and 4 for all of the different types of signals considered here (and all kinematic parameters in both PMv and MI, so for all 256 instances), using an average-selection approach (see METHODS). For this analysis, we selected a random set of inputs (from each area) independently with replacement 100 times, and then plotted the mean decoding performance across those 100 sets. For visualization, we averaged results across 8 kinematic parameters, 2 monkeys, 2 sessions, and 2 areas (MI and PMv) in Fig. 5, *A* and *B*. We found that on average, when using <6 channels, the LF, H1, and H2 signals' performances were not significantly different from SA performance (Fig. 5*A*). However, with increasing channels (Fig. 5*B*), the mean *r* using SA was significant at 6 inputs over H1, at 10 inputs over LF, and at >16 inputs over H2 (assessed with a 2-sample *t*-test: right tail, $P < 0.05$). By comparison, the greedy case, which selected for optimal channels, on average yielded SA > H2 > LF or H1 for all numbers of input (Fig. 5*C*; except H2 > H1 at ≥2 inputs). Furthermore, the greedy case always performed better than the average-case approach, indicated by all points being above the diagonal in Fig. 5*D*. In addition, the greedy approach produced an earlier peak, reflecting that fewer inputs were necessary to achieve optimal performance compared with the average approach (Fig. 5, *E* and *F*).

Our goal is to assess the maximum potential information that might be extracted from each signal type and from combinations of these signals. One simple option would be to include all of the inputs in the fitting of a given decoder, e.g., all of the recorded single units when building a spike decoder. However, a decoder using smaller subsets of units or channels can potentially outperform the full set, because of overfitting the training data in the latter case. We therefore adopted a greedy approach for the selection of subsets of inputs that provide optimal performance. (An exhaustive search of all of the possible combinations is not feasible in practice.)

We further examined whether our results were dependent on type of decoding algorithm (e.g., Kalman filter vs. a hidden-state model) or parameters such as the window size over which the neural signal was averaged (150 ms). For comparison, we used a hidden-state model decoding algorithm (Vargas-Irwin et al. 2010) and different window sizes (50, 150, 250, 350, 450, 550 ms) but found that the relative ranking of the different signals remained the same as our findings in Fig. 5*C* (data not shown). We also briefly explored whether a nonlinear algorithm [support vector regression (SVR)] would change the relative performance of the different signals. In *monkey C*, for one session, even though we observed an overall improvement when using SVR instead of the Kalman filter, the relative ranking of the signals was similar on average. Performing the SVR decoding on all sessions was computationally prohibitive given our greedy-selection approach under an *n*-fold cross-validation scheme. Thus, for the remaining analysis combining information across areas and/or signals, we proceeded with the Kalman filter best-case "greedy" approach as it provided the optimal trade-off between runtime computational complexity and decoding performance.

Decoding Performance Plateaus When Combining Areas and Signals at the Level of the Better Area or Best Signal Performance

In the remainder of this study, we performed several analyses with the aim of combining inputs across areas and across signal types to exploit potentially independent information across areas and across signals. For example, if PMv and MI carry somewhat independent information about reach and grasp, selecting signals from both areas should improve decoding performance; on the other hand, if information is mostly overlapping, minimal improvement should be observed. We tested this by building MA decoders based on the same signal drawn from pooling data across MI and PMv. We compared decoding performance of the MA decoder to that of the single-area-based decoder that gave the better performance. Independent information could also be present across signal types. Therefore, we also considered the effect of combing multiple signal types from both MI and PMv. Although not physiological, this approach can help define the best performance when

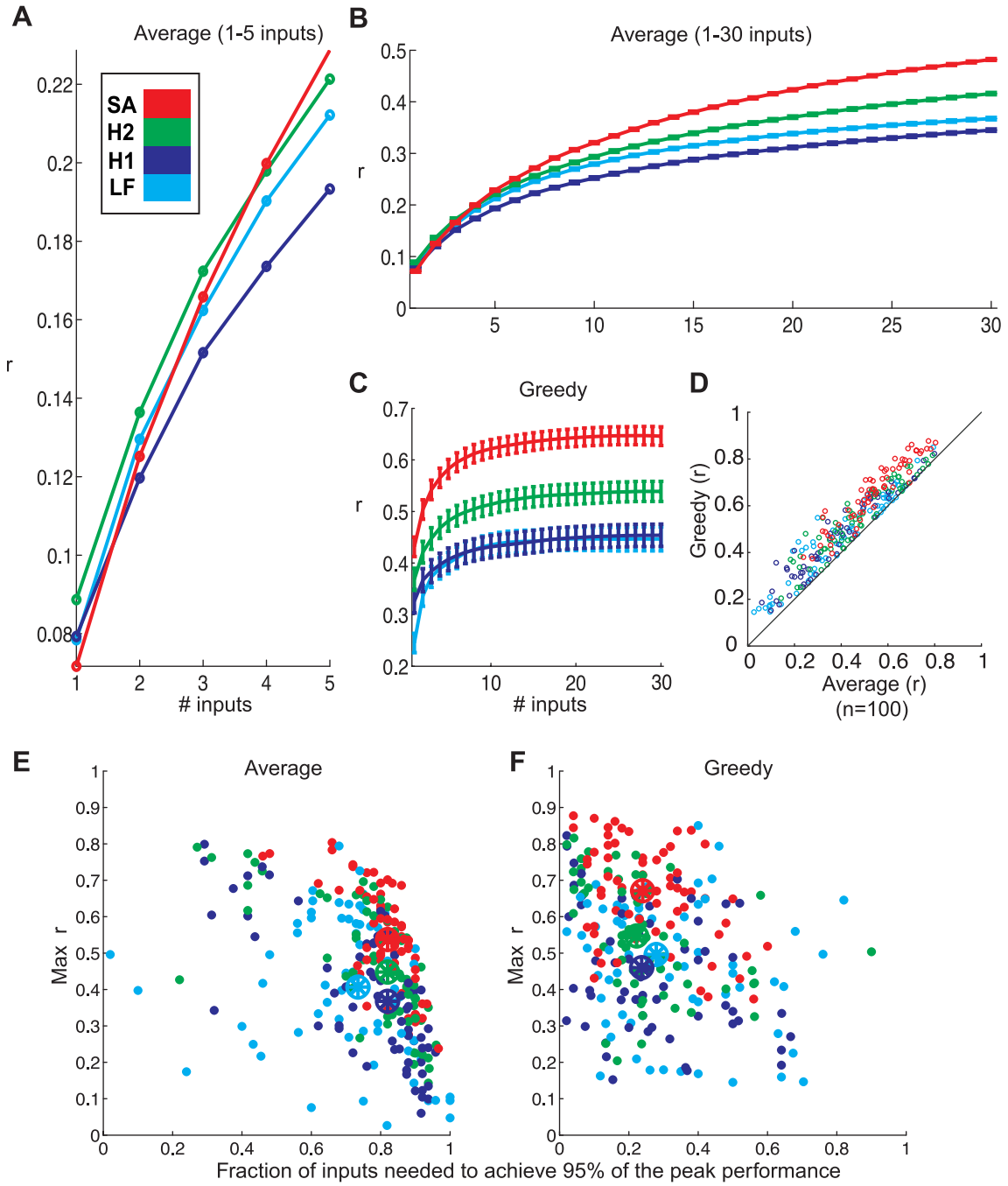

Fig. 5. Comparison of greedy-selection decoding vs. average-case decoding. *A* and *B*: comparison of decoding performance using an average-case approach (see METHODS) instead of the greedy-selection approach used in previous figures for 1–5 inputs to highlight the relationship in the mean decoding performance between the signals (*A*) and 1–30 inputs to demonstrate the relationship with larger numbers of inputs (*B*). Note that for very few inputs (<4), average decoding performance based on LFPs is not significantly different from that based on spikes, but with ≥17 inputs spikes outperform LFP-based decoders. *C*: similar comparison using a greedy-selection approach. Note that spikes outperform LFP-based decoders at all numbers of inputs. *D*: comparison of the best performance using the average-case approach and the greedy approach for the same data (comparing data for 8 kinematic parameters, 4 signal types, 2 areas each in 4 sessions). Note that all points are above the diagonal, indicating that the greedy approach performed better than the average-case approach. *E* and *F*: fractions of inputs required for each reconstruction to attain 95% of its maximum correlation coefficient achievable with up to a maximum of 50 inputs vs. maximum correlation coefficient for average (*E*) and greedy-selection-based (*F*) decoding. Starred markers represent medians on each axis for each signal. Note that the lower fractions of inputs for the greedy-selection-based decoding indicate that maximal decoding performance is achieved with fewer inputs with the greedy approach compared with the average-case approach.

multiple signals available from an intracortical electrode array are considered. For this analysis, we built decoders using just LFP signals, termed the multiband local field potential (*mb*-LFP) decoder, or combinations of all signals including spikes and LFPs, termed the hybrid signal (HS) decoder.

Figure 6 shows examples of decoding for *z*-position and grip aperture combining signals from both areas, spikes (MA spikes), all three field potential bands (*mb*-LFP), or all signals (HS), to give a qualitative presentation of the benefits of combining areas or signals for the same time segment as in Fig.

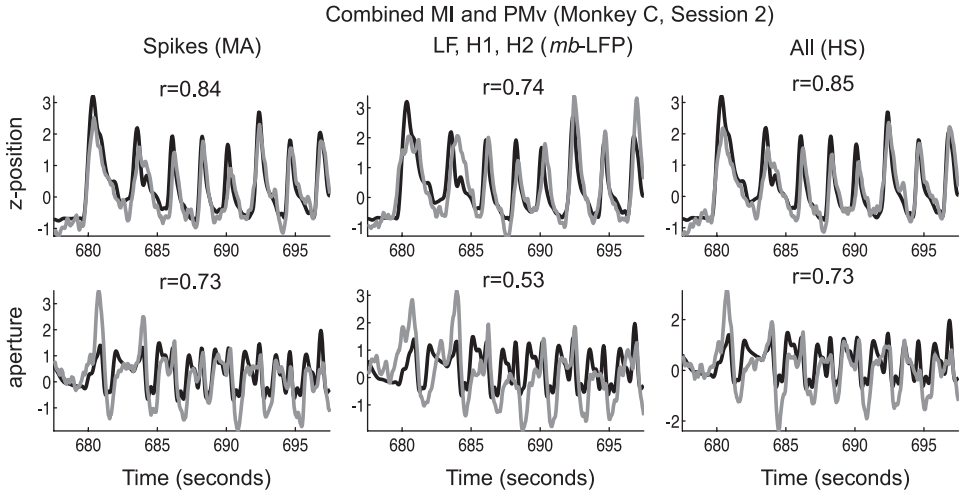

Fig. 6. Examples of hybrid decoders. This figure illustrates the effect of using from both areas MI and PMv, optimal combinations of spiking activity [multiarea (MA) spikes], only multiband LFPs (*mb*-LFPs), or SA and *mb*-LFPs [hybrid signal (HS)]. Examples of true and decoded *z*-position and aperture are shown for the same time segment as displayed in Fig. 2. Original kinematics in black, decoded in gray. *r* values were computed on the entire reconstruction for each parameter and not just for the time segment displayed here.

2. Because decoding saturates at ~30 inputs and large ensembles entail high computational costs, we limited ensemble size to a maximum of 50 inputs, selected with the greedy procedure from the total pool (see METHODS). Next, we summarized the decoding performance using the MA, *mb*-LFP, and HS approaches (Fig. 7; Table 3.1, 3.2). When combining a signal type using two areas (Fig. 7, *bottom* 4 bars for each kinematic parameter;), the general rank-order trend between the signals (i.e., LF < H2 < SA) was still observed. Spiking, on average, provided 14% higher *r* than the next best signal, H2.

Next, we compared MA, *mb*-LFP, and HS decoders' performance to single-area, single-LFP band, and single-band decoders, respectively.

Improvements (Δr) when combining areas. If MI and PMv were to contain independent information, then combining a signal type across both areas should substantially improve decoding performance. Hence, we quantified the improvements in combining the same signal type across areas versus using just one area. We found that the improvements in *r* when selecting the best ensembles from the pool of MI and PMv data (vs. the better of these 2 areas) were significantly greater than zero for each signal band, but very small ($\Delta r = 0.03 \pm 0.03$; Fig. 8*A*, Table 3.3), suggesting that the reach and grasp information across areas was similar. However, when comparing the improvement of MA decoding over using the signal from the single area that individually gave the lower decoding performance of the two areas, we found that the improvement in *r* could be more substantial and significant ($\Delta r = 0.15 \pm 0.08$; Fig. 8*B*, Table 3.4). Comparison to the "better" or "worse" area was performed for each decoding instance because no one area (MI or PMv) was consistently better than the other (Fig. 4, *E* and *F*).

Improvements (Δr) when combining LFP signals. Similar to the approach used in the previous section, the independence of information represented in the LFP bands can be evaluated by measuring the improvement in decoding performance when LFP signals are combined. Hence, we used signals from both areas and compared decoding quality when combining LFP bands (*mb*-LFP) to using any single band. Improvements were largest when the *mb*-LFP signal was compared with the LF band ($\Delta r = 0.16 \pm 0.17$) and smallest for the H2 band ($\Delta r = 0.05 \pm 0.05$) (Table 4.1). We mentioned above that LF on average performed better than the H1 band for velocity and H1 and H2 bands performed better than the LF band for position (Table 2.2, 2.3; Fig. 4, *A* and *B*). Thus one might predict that combining LF, H1, and H2 bands should considerably improve position decoding for LF and velocity decoding for H1. As seen in Table 4.2 and 4.3, combining LFP bands allowed the pooling of information across LF, H1, and H2 bands to achieve more consistent decoding across both position and velocity parameters. Improvements by pooling suggest that each band contains unique kinematic information not available from the other bands. However, on average combining LFP bands still gave 0.04 ± 0.01 worse *r* than using spikes from both areas.

Improvements (Δr) when combining spikes and LFPs. Finally, we evaluated the independence of information represented in the LFP bands and spiking signals by measuring the improvement in decoding performance when combining LFPs and spikes. Hybrid decoders produced a small, but significant, improvement versus using spikes alone (0.02 ± 0.03; Table 4.5). Stated differently, when combining LFP with spikes, the *r* saturates at a level just 0.02 over that achieved by spiking alone, suggesting that the information in LFPs was largely, but not entirely, contained within spiking information. The hybrid decoder was slightly better than the *mb*-LFP decoder (0.06 ± 0.01) or spiking alone, but considerably better than single LFP bands (Table 4.5).

Is There a Bias in PMv for Grasp Information?

The results so far revealed no significant difference between MI and PMv in the decoding performance of any kinematic parameter (including grasp aperture) when comparing data over all sessions across both monkeys (Fig. 4; Table 5.2, 5.3). On the other hand, prior work suggests that PMv may preferentially encode grasp parameters compared with MI (Kurata and Tanji 1986; Rizzolatti et al. 1988; Umilta et al. 2007). When comparing MI and PMv decoding performance for each individual monkey, we found that MI decoding performance (*r*, averaged across kinematic parameters) in *monkey C* was 21% better than that in *monkey G* (and 16% better than PMv performance in *monkey C*), while PMv performance in *monkey G* was 27% better than that in *monkey C* (and 32% better than MI performance in *monkey G*). In *monkey C*, *x*-velocity was on average consistently better decoded in MI compared with PMv (MI: 0.46 ± 0.04; PMv: 0.30 ± 0.04), but the decoding performance of other kinematics parameters when considered

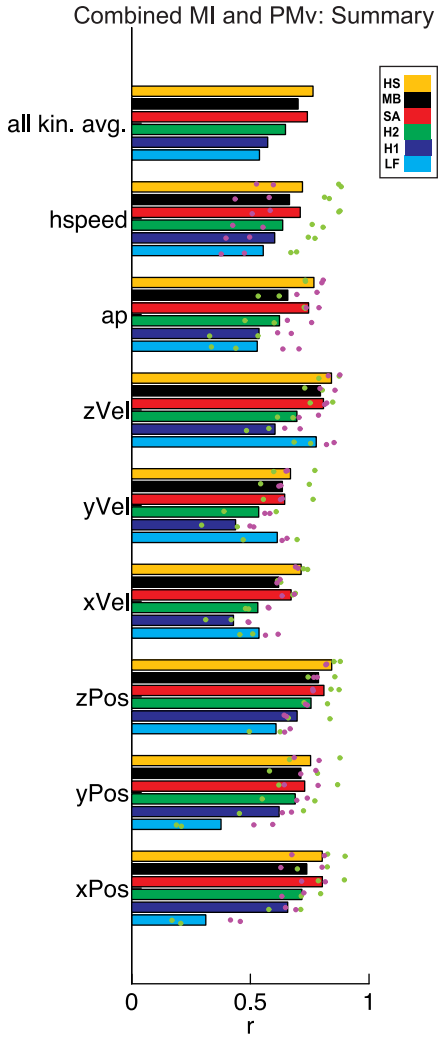

Fig. 7. Summary of hybrid decoding. Decoding performance when pooling the same type of signal across MI and PMv or using all (LF, H1, and H2) field potentials (MB) or all signals (HS) from both areas in 2 monkeys (*monkey C*, light green; *monkey G*, magenta).

individually was not significantly different between MI and PMv. It is unclear whether these results reflect variability in the organization of information in MI and PMv across monkeys, or if they merely reflect sampling biases for limited ensemble sizes (also note *monkey G*, *session 2* decrease in number of units; Table 1) and compositions randomly detected by the fixed electrode array. Nevertheless, in our sample of two monkeys, there was no consistent bias for PMv or MI preferentially encoding grasp or any other decoded parameter such as position or velocity.

Biases in representation between PMv and MI were also evaluated by comparing whether a greedy algorithm would select more inputs from PMv when decoding aperture and more inputs from MI when decoding reach. Although there was a general bias such that PMv H1 and spiking signals were chosen more often than MI signals, this effect was mostly due to *monkey G* (Table 6). We did not find significant differences in this input selection bias between aperture and the reach parameters when using the MA, *mb*-LFP, or HS decoders (unpaired 2-sample *t*-test, $P > 0.1$; Fig. 9).

Spikes are the Dominant Contributor in Hybrid Decoding

Do greedy algorithms select greater fractions of one signal type? We hypothesized that LFPs might significantly contribute in hybrid decoders by dominating the fractions of inputs selected in the HS pool. Contrary to this hypothesis, we found that large fractions of inputs selected for inclusion in hybrid decoders were spiking units (Fig. 9*C*, Fig. 10*A*; mean fraction across sessions, monkeys, and kinematic parameters: 0.56 ± 0.03). However, we did find that small, but consistent, fractions of the signals in the optimal subset selected by the greedy method were LFPs (mean fraction of LFP channels selected, averaged across sessions, monkeys, and kinematic parameters: LF 0.12, H1 0.13, H2 0.19) Thus, even though the accuracy for the HS decoder saturated at the level of spiking-based performance, LFP input channels did contribute toward the decoding (Fig. 9*C*, Fig. 10*A*). In addition, in the decoders using *mb*-LFP bands, the fractions of inputs of each type were biased in favor of H2 inputs over H1 and LF inputs (Fig. 9*B*; Table 4.4).

Although spiking channels dominated the HS pool, LFPs constituted the majority in the HS pool for 7 of 32 instances (4 sessions × 8 kinematic parameters). Most of these (6/7) occurred for *monkey G*, *session 2*, during which the numbers of spiking units were lower in both MI (to 30 units, −47%) and PMv (to 108 units, −37%). (The other instance was *monkey C*, *session 1* for *x*-position). However, a LFP band (H2) had performed better than spike-based decoding (of *y*-position and aperture, by 9% and 3%, respectively) for only two of these six instances. Furthermore, in three of four sessions (across monkeys) for decoding *x*-position, the majority of inputs in the HS pool were LFP channels, even though when the signals were used individually (LF, H1, H2, or spiking ensembles) spiking inputs achieved the highest performance (Fig. 7). For other kinematic parameters, in at least three of the four sessions, spikes were the majority input in the HS pool. These examples illustrate that the fraction of inputs, when combining input signal types selected with the greedy process, only provides an indirect measure of signal performance as it does not reveal the

Table 3. *Results for multiple-area decoding*

Signal/Comparison	1. Mean *r* (MA, combined areas)	2. Mean RMSE (MA, combined areas)	3. Mean *r* Improvement (using both areas over just the better area)	4. Mean *r* Improvement (using both areas over just the worse area)
Statistical test/notes	Mean sig. diff. (all pairs)	Mean sig. diff. (all pairs)	*t*-Test for mean sig. diff. from zero	*t*-Test for mean sig. diff. from zero
LF	0.54 ± 0.03 (†H1) (‡H2) (*SA)	0.20 ± 0.04 (†H1, H2) (*SA)	0.02 ± 0.02*	0.11 ± 0.07*
H1	0.57 ± 0.02 (†H2) (*SA)	0.19 ± 0.03 (†H2) (*SA)	0.03 ± 0.03*	0.19 ± 0.09*
H2	0.65 ± 0.02 (‡SA)	0.18 ± 0.03 (‡SA)	0.03 ± 0.03*	0.17 ± 0.08*
Spikes	0.74 ± 0.02	0.15 ± 0.03	0.02 ± 0.03*	0.14 ± 0.07*
All signals	0.62 ± 0.01	0.18 ± 0.04	0.03 ± 0.03*	0.15 ± 0.08*

Conventions similar to Table 2. MA, multiarea decoding.

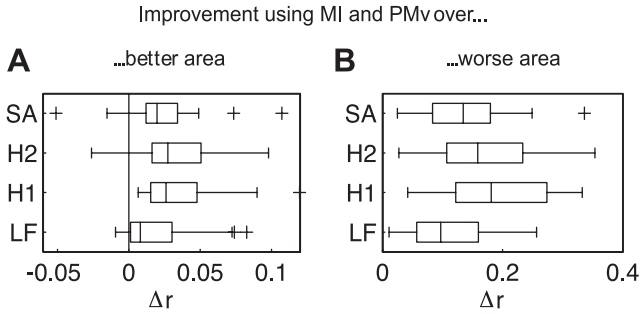

Fig. 8. Improvements when using multiarea (MI and PMv) decoders. *A*: improvement in decoding performance (Δr) when pooling across areas (MA) vs. the better of MI and PMv decoding performance for each signal in each session (mean ± SE: 0.03 ± 0.03). *B*: improvement in decoding performance when pooling across areas (MA) vs. the worse of MI and PMv decoding performance for each signal in each session (0.15 ± 0.08). Note that the improvement compared with the worse area is significantly greater than the improvement compared with the better area. Note also that the better area could be either MI or PMv for each session/monkey/kinematic parameter and neither area was always better (see Fig. 4, *E* and *F*). Each plot is a box and whisker plot. The box represents the 25th and 75th percentile range of the values obtained for r across monkeys, sessions, and kinematic variables. The line inside the box represents the median, and the whiskers extend to $\pm 2.7\sigma$, or up to points not considered outliers (which in turn are plotted as plus signs).

magnitude of decoding improvement each signal contributes. We examine this next.

Relative contribution of LFPs vs. spiking units in hybrid decoding. Even though LFPs did not constitute the majority of the inputs in the hybrid pool, it was possible that they may have had a disproportionate contribution toward the improvement of r compared with spiking signals. To clarify this issue, we compared the relative contributions of spiking units and LFP channels to the overall reconstruction performance. Consequently, we adopted the following strategy: We split the pool of all inputs used for HS into the 10 inputs providing the initial best decoding performance and the up to 40 remaining inputs. Figure 10*A* plots the order in which signals of different types were added to the pool of signals used for decoding. Spiking units tended to be the dominant signal type in the first 10 inputs that were added with the greedy procedure (mean across kinematic parameters, sessions, and monkeys: 68% in the first 10, 53% in the next 40; see Fig. 10*A* for comparison by signal and Fig. 10*B* for comparison by area). Next, we compared the decoding accuracy obtained with the best 10 inputs (Table 5.1) versus the 50 best inputs. Most of the improvement was with the first 10 inputs (mean improvement with first 10 inputs vs. last 40 inputs, averaged across kinematic parameters, sessions, and monkeys: 0.70 ± 0.02 vs. 0.06 ± 0.01). This suggests that even though there were signals from LFP bands contributing in the pool of all signals, their contribution was smaller. However, the 32% LFP inputs in the top 10 of the HS ensemble indicate that there were some LFP inputs that outperformed spiking units in their contribution to the greedy-selection-based decoding.

In summary, these results demonstrate that spiking contributes the majority of the decoding gain when combining all types of inputs. Furthermore, combining all signals improves decoding by only ~3% versus using spiking. Spiking inputs constitute 68% of the top 10 of ensemble sizes up to 50 when combining all signals, and the top 10 inputs achieve 92% of the maximum performance. The maximum improvement of a hybrid decoder over one using only spikes was just 9%. Even though LFP signals contribute in the top 50 channels used, they fall largely in the flat portion of the "greedy curves," showing that the relative improvement by using these LFP signals is minimal.

Correlation among signal types. We also briefly examined the correlation coefficient among LFP channels in different frequency bands and among spikes (among all pairwise channels or units within each area). We found that the LF band was most highly correlated ($r = 0.79$), followed by the H1 band ($r = 0.48$) and the H2 band ($r = 0.46$). Spikes were less correlated than any of these LFP bands ($r = 0.14$).

DISCUSSION

This study demonstrates that although different LFP frequency bands and spikes relate to different ongoing processes and could carry complementary movement information, reach and grasp information added by various LFP frequency bands is typically less than and primarily contained within that already available in SA ensembles. Spikes typically outperform LFPs in reconstructing the kinematics of free reach and grasp actions, resolving inconsistent results in the field. This finding is based, for the first time to our knowledge, on a naturalistic 3D reach and grasp task, dual-area 96-multielectrode array recordings, and computationally intensive greedy-selection-based decoding applied to a broad range of neural signals including spikes, low- and high-frequency LFPs, and MUA in high-frequency broadband LFPs. Furthermore, although previous studies using somewhat indirect approaches suggested a bias for grasp representation in PMv signals (Kurata and Tanji 1986; Rizzolatti et al. 1988; Umilta et al. 2007), we show directly that both reach and grasp can be similarly reconstructed from small, local neuronal populations

Table 4. *Results for multiband LFP and hybrid signal decoding*

Signal/Comparison	1. Mean r Improvement (using all LFP bands vs. just 1)	2. Mean r Improvement [using all LFP bands vs. just 1 (position)]	3. Mean r Improvement [using all LFP bands vs. just 1 (velocity)]	4. Mean Fraction of Inputs of Each Type in *mb*-LFP Decoding	5. Mean r Improvement (using all signals vs. just 1 signal)
Statistical test/notes	t-Test for mean sig. diff. from zero	t-Test for mean sig. diff. from zero	t-Test for mean sig. diff. from zero	Mean sig. diff. (all pairs)	t-Test for mean sig. diff. from zero
LF	0.16 ± 0.17*	0.31 ± 0.18*	0.04 ± 0.06*	0.22 ± 0.03 (†H1) (*H2)	0.22 ± 0.18*
H1	0.13 ± 0.08*	0.09 ± 0.05*	0.19 ± 0.07*	0.30 ± 0.02 (*H2)	0.19 ± 0.10*
H2	0.05 ± 0.05*	0.03 ± 0.02*	0.10 ± 0.04*	0.48 ± 0.02	0.12 ± 0.07*
Spikes					0.02 ± 0.03*
All signals	0.11 ± 0.12*	0.14 ± 0.16*	0.11 ± 0.09*		0.14 ± 0.13*
					0.02 ± 0.02 (compared to best)

Conventions similar to Table 2. *mb*-LFP, multiband LFP.

Table 5. *Results for top 10 inputs in hybrid decoding or only MI or PMv inputs*

Signal/Comparison	1. Mean *r* (top 10 inputs only)	2. Mean *r* (MI only)	3. Mean *r* (PMv only)
Statistical test/notes	Mean sig. diff. (all pairs)	n/a	n/a
LF	0.44 ± 0.02 (†H1) (‡H2) (*SA)	0.46 ± 0.03	0.49 ± 0.03
H1	0.43 ± 0.02 (‡H2) (*SA)	0.43 ± 0.03	0.50 ± 0.03
H2	0.51 ± 0.02 (*SA)	0.53 ± 0.02	0.56 ± 0.03
Spikes	0.62 ± 0.02	0.65 ± 0.03	0.67 ± 0.02
All signals	0.50 ± 0.01		

Conventions similar to Table 2. n/a, Not applicable.

in either MI or PMv for this naturalistic task, which also has grasp complexity comparable to tasks used in previous studies. In an applied context, the results demonstrate the general superiority of spike-based population decoding overall, but also show that multiband LFP signals are nearly as good. These findings suggest that both spikes and various LFP frequency bands collected from intracortical sensors can be useful sources for human BCI command signals (Ajiboye et al. 2010). These neural signals can to some degree substitute for each other, adding potential robustness to BCIs based on intracortically recorded signals. The results also suggest that MI and PMv could provide similar command signals on average to generate naturalistic reach and grasp actions for BCI applications, but they do not determine whether this similarity would apply for other types of hand or reaching tasks.

In our previous work (Bansal et el. 2011), we focused on the information in low-frequency LFPs (LFs). We did not examine the advantages of combining the same class of signal from MI and PMv or combining from both these areas different classes of signals: LF, H1, and H2 bands and SA. Because of the focus on LFs, our analysis of the greedy- and average-selection approaches was restricted to just 4 of a possible 256 instances (256 instances = 2 monkeys × 2 sessions × 2 areas × 8 kinematic parameters × 4 signals) in that study. In addition, a comparison of relative information in LF, H1, H2, and SA based strictly on our three previous studies (Bansal et al. 2011; Vargas-Irwin et al. 2010; Zhuang et al. 2010) would be hindered by the different choices of algorithms, parameters, etc., made in each of these studies. Thus, besides addressing hybrid decoding, in the present study we kept the decoding algorithm and parameters the same when decoding using each signal to facilitate this comparison.

Spikes as Optimal Signals

Spiking in neuronal ensembles typically outperformed multichannel, multiband LFP signals in decoding 3D kinematic parameters. We conclude that this effect was not simply a reflection of our decoding approach, or the choice of *r* or nRMSE as the optimization measure in the greedy selection of channels and signal types. In addition, the superiority of spikes was not highly dependent on the greedy algorithm itself because similar results were obtained with the average-selection method as long as populations typically comprised >16 units. Combining spikes and LFPs across areas only marginally improved decoding performance over using only spikes but did increase decoding performance substantially over that achieved by using LFPs alone. This is consistent with the interpretation that kinematic information in LFPs is largely contained within that already available in neuronal ensemble spiking.

The differences in decoding performance based on spikes and LFPs contrasts with previous studies, which used single-electrode recordings (or at most 16 electrodes within a session) and averaged results across days. In one set of studies, LF decoding exceeded spiking (Mehring et al. 2003) and *hf*-LFPs (Rickert et al. 2005), and in another study MUA yielded a higher decoding performance than LFs and SA (Stark and Abeles 2007). These results seem, in part, to be counterintuitive, because if neurons are the output that ultimately generate movements and control kinematics, then one would predict that SA information would best capture details of kinematics. Our data show that these discrepancies are largely a consequence of sample size: The ranking of signal success is dependent on the number of units/channels used in the decoder. We demonstrate that LFPs can contain more information than spikes when relatively small numbers of units are used, consistent with this earlier work. To explain this result, consider, for example, decoding of wrist position in the following scenario. Wrist decoding would be worse when using spiking from a single unit that is only correlated with elbow joint angle, compared with a more global LFP signal that contains some wrist information. However, when many spiking units become available, the likelihood of finding cells that are tuned for wrist decoding would increase and for some large enough neuronal ensemble the decoding performance would exceed that achieved by using FP signals alone. Our data in Fig. 5, *A* and *B*, support this scenario. The fact that the greedy algorithm was

Table 6. *Fractions of PMv inputs by signal for MA decoders*

		Monkey C		*Monkey G*	
	Mean	S1	S2	S1	S2
LF	0.56 ± 0.03	0.52 ± 0.01	0.51 ± 0.02	0.46 ± 0.05	0.73 ± 0.07
H1	0.60 ± 0.02*	0.55 ± 0.03	0.59 ± 0.05	0.60 ± 0.05	0.66 ± 0.05
H2	0.54 ± 0.03	0.50 ± 0.03	0.61 ± 0.05	0.50 ± 0.06	0.53 ± 0.07
SA	0.60 ± 0.03*	0.46 ± 0.05	0.47 ± 0.04	0.66 ± 0.04*	0.83 ± 0.02*

Values are means ± SE over kinematic parameters (*t*-test for significant difference from 0.5; *$P < 0.01$). The range of mean fraction of PMv inputs was 0.46–0.83. S1 and S2, *sessions 1* and *2*.

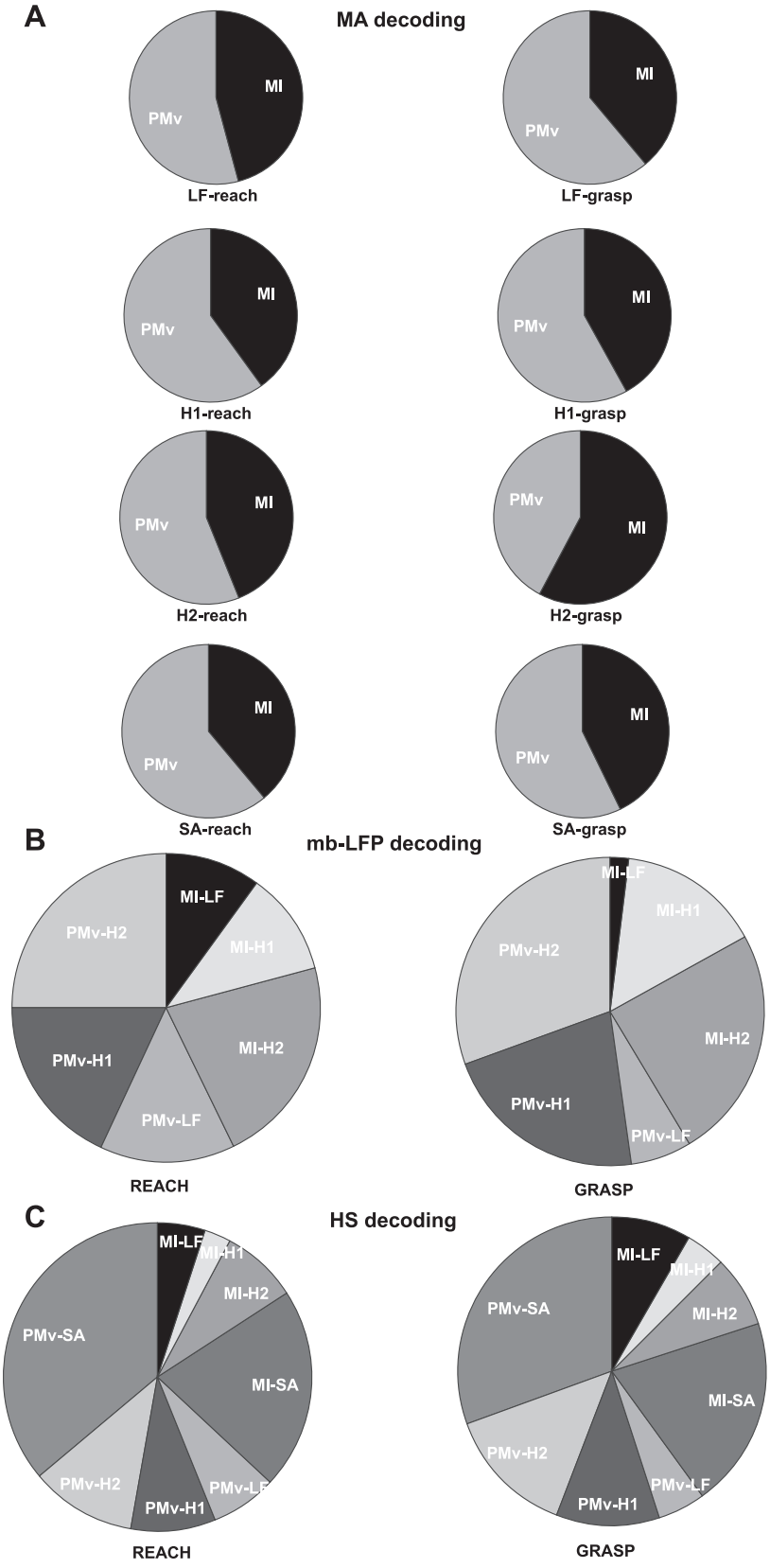

Fig. 9. Fractions of inputs of each type of signal from each area in the optimal pool of input signals used for decoding. Fractions of inputs across all kinematic parameters that came from PMv vs. MI in the multiarea decoder (MA) for each neural signal (*A*), all field potential bands-based decoder (*mb*-LFP; *B*), or all signals-based decoder (HS; *C*), for a maximum pool of 50 inputs that were tested with the greedy procedure. Pie chart plots the mean proportion of each type of signal (out of all selected signals) selected by the corresponding decoder. Reach refers to the average fractions obtained for decoding across *x*, *y*, and *z* positions, *x*, *y*, and *z* velocities, and hand speed. Grasp refers to similar average fractions for decoding aperture. A slight overall bias for PMv spikes for both reach and grasp was observed, in part due to the reduced number of units in *monkey G*, MI, *session 2*. However, there were no differences in this bias for reach vs. grasp.

consistently better when using spikes than when using other signal types is explained by the selective nature of that algorithm: It identified for each step the very best neuron out of a larger pool of possible choices (Fig. 5*C*). This reasoning predicts that the decoding differences observed here [i.e., SA > H2 (MUA) > LF] could become more evident with larger-scale recordings where the selection is larger. This assertion is also supported by our observation that spiking units were

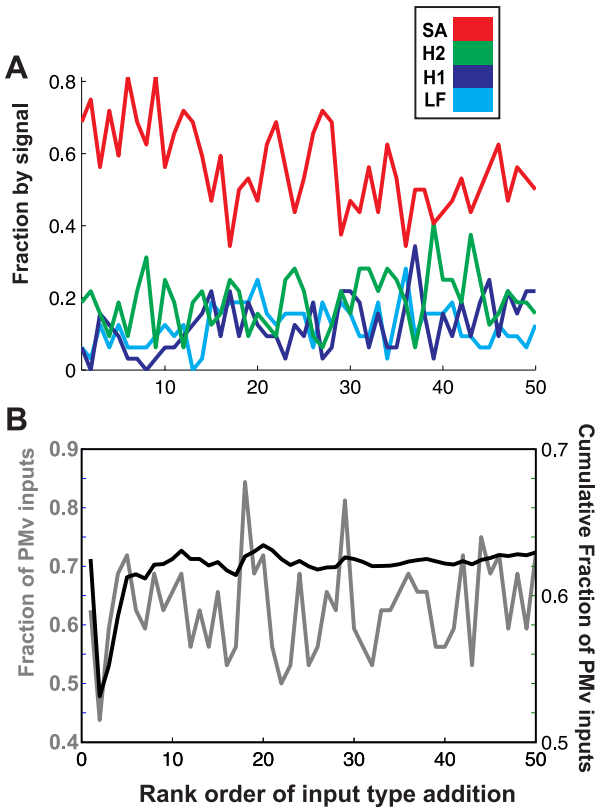

Fig. 10. Composition of the optimal input pool for hybrid signal (HS) decoding by signal type and cortical area. The order in which the inputs were added to the HS pool to decode each signal for each session with the greedy-selection algorithm (see METHODS) is shown. *A*: summary of fractions of inputs of each signal type added at each rank. *B*: summary of fractions of inputs added at each rank from PMv (gray) and the corresponding cumulative fraction of PMv inputs added (black).

generally less correlated than any LFP band, and could therefore potentially add more independent information with increasing number of units. Note also that our electrode arrays allow for no bias in selection, so that these results reflect the available information from an arbitrary pool of cells within a small (4 × 4 mm) region of MI or PMv.

Nature of Signals

LFPs have been associated with cortical inputs, while spikes are output. Based on this oversimplified view, a comparison of these signals could potentially reveal the input-output transformations performed by a cortical area. Insofar as LFPs reflect inputs into an area, their lower decoding performance could thus reflect differences in information between the input and output in PMv and MI. However, there are many issues that make it difficult to relate LFP to simple inputs to an area. For example, LFP reflects input but also dendritic processing, which is "diluted" by the spatial averaging of synaptic currents inherent in extracellular recording (Rasch et al. 2008). Intracellular recordings would be required to measure input currents on a single-cell basis. Spikes are recorded extracellularly from single neurons, but it is important to recognize that spikes likely reflect intrinsic processing as well as the output of an area because cortical neurons have extensive recurrent axonal networks. These features of spiking and fields complicate inferences about input-output transformations that the signals reflect.

Our data agree with previous suggestions (Logothetis 2002) in that H2 may primarily reflect the spiking of a collection of cells (MUA) because decoding performance of H2 and spiking was generally similar. Nevertheless, H2 could also contain other fast synaptic components. Our filter settings during recording limited the LFP bandwidth to 0.3–500 Hz, which removed discriminable single units from this band. Thus we cannot determine whether movement information available in H2 was related primarily to spiking or synaptic currents. On the other hand, power in the H2 band averaged over small time windows as done here has similarities, from a signal processing view, to what Stark and Abeles (2007) called MUA. By contrast, Mehring et al. (2003) defined MUA as thresholded but unsorted neuronal spikes [referred to as multiple single units in Stark and Abeles (2007)], while MUA in Stark and Abeles consisted of root-mean-squared high-pass-filtered potentials. Thus comparisons with MUA-based decoding require a careful analysis of the actual signal employed. The relative performance of decoders based on sorted (our SA signal) or thresholded but unsorted spikes (Chestek et al. 2009) is a subject of ongoing research for BCI applications.

Among the FP signals analyzed in this study H1 was generally the worst for decoding. H1 might reflect more of a contribution by LFPs and less of spikes. Work by other groups (Belitski et al. 2008; Rickert et al. 2005) and ours (Zhuang et al. 2010) has observed a trend that the predominant information about stimuli or motor responses occurs in the low- and high-frequency LFPs, with a reduced information content in the middle-frequency bands (beta band, cf. introduction). Consistent with this idea, middle-frequency bands as considered for the same data in Zhuang et al. (2010) performed even worse. We did not consider midbands in the present study because of this known poor performance.

Comparison of MI and PMv

Surprisingly, we found roughly the same amount and type of information about reach and grasp in PMv and MI neuronal populations, although the better of the two areas differed between the monkeys. To our knowledge, this is the first demonstration that PMv contains continuous 3D reach and grasp kinematic information in SA and H1 and H2 bands and is the first comparison between PMv and MI. Our results suggest that the information in PMv and MI about both reach and grasp is overlapping, because decoding improved marginally if at all when the two were combined (see also Bansal et al. 2011). These results are remarkable because previous studies have indicated that PMv is dominated by signals related to grasping (Kurata and Tanji 1986; Rizzolatti et al. 1988; Umilta et al. 2007), while MI contains both grasp and reach information in small local ensembles (Vargas-Irwin et al. 2010). We suggest three possible explanations. First, our task required continuous naturalistic movements and updates that may engage networks in different ways than the more sequentially or discretely organized and stereotyped tasks used in previous studies for either MI or PMv. Other studies have suggested that PMv neural properties may be subject to context (Fluet et al. 2010; Xiao et al. 2006). Second, our decoding approach extracted kinematic information from any possible set of cells in

the recorded neural ensemble, whereas previous approaches (Kurata and Tanji 1986; Rizzolatti et al. 1988; Umilta et al. 2007) quantified fractions of individual cells that were best tuned to either reaching or grasping. We might therefore have obtained significant kinematic information even from a minority of tuned cells in one area, which with a large enough sampled population can achieve similar decoding performance compared with another area with a larger fraction of tuned cells. This sort of distributed coding has been previously demonstrated in MI, PMd, and other cortical areas, but this is the first comprehensive comparison of ensembles across MI and PMv (Bansal et al. 2011; Carmena et al. 2003; Nicolelis and Lebedev 2009; Wessberg et al. 2000). Also note that single-cell studies select recorded cells, while we did not. Third, our electrodes sampled only from the cortical surface representation of MI and PMv, and may not be representative of the properties of cells deeper in the arcuate or central sulci. However, to the best of our knowledge, reach and grasp neurons have been reported both on the surface and in the depth of the arcuate sulcus, with no clear organization of reach- versus grasp-preferring neurons with depth (Stark et al. 2007). The fixed ~1-mm length of the electrodes also restricts us to sampling around the layer 3/5 boundary in MI and PMv. While the representation in cells and LFP signals might change in different layers, there is no evidence for this conjecture. In summary, our results suggest that the nature of information in PMv could depend on task types or other variables, which may explain recent conflicting views of motor cortex representation (Graziano and Aflalo 2007).

Since we used anatomical landmarks (see METHODS) for placing electrodes, we cannot completely rule out the possibility that our PMv electrodes straddled PMd, which might make the observed lack of difference in reach and grasp encoding less surprising. However, in one monkey we explored the region further ventral to the locations of the PMv implants in this study and found no arm or hand representation, but only a face representation. Within the PMv array, we found no clustering of reach along more dorsal electrodes or grasp along the ventral electrodes. These observations suggest that we are not straddling PMd.

Implications for BCI Applications

Our results suggest that when recording from ensembles of neurons (e.g., via 96-channel microelectrode arrays), spiking signals are the richest signal source of motor commands for BCI applications. However, this conclusion is conditioned on the number of units used. For very small ensembles, LFP signals could provide a better command signal because single units might be more restricted in their information content. While this hypothesis requires testing in BCI applications, results of open-loop decoding have guided decoding approaches in prosthetics research using both able-bodied monkeys and humans with paralysis. Thus our results provide important guidance for neuroprosthetics that aim to restore movement ability in people with paralysis using intracortical LFP or spiking signals.

One implication of our results is that the many different signals available on an intracortical array may be useful to ensure longevity. Spikes may be stable only across days to weeks, and even then only for a subset of channels (Chestek et al. 2009; Dickey et al. 2009), necessitating the frequent updating of decoding filters (Hochberg et al. 2006). On an array where the number of spiking units is small or decreases over time, LF, H1, and H2 signals may provide a substitute signal to create a robust decoder. LFPs may provide other advantages as BCI signal sources such as signal and tuning stability across several months (Chao et al. 2010), while recorded SA and its properties might change across days because spike sampling is sensitive to small motions of the electrode.

Learning might be another way to enhance BCI control, and it may be possible to learn to control some signals better than others. There is considerable evidence that spiking can be modified through learning (Carmena et al. 2003; Fetz 1969; Ganguly and Carmena 2009; Moritz et al. 2008), but it is not clear whether individual LFP bands are more or less readily adaptable in BCI applications (Nowlis and Kamiya 1970; Pfurtscheller et al. 2010; Plotkin 1976; Wolpaw and McFarland 2004). It is also not clear how well each of these signals is amenable to volitional control in a closed-loop setting. The comparison of LFP, spike, and hybrid decoders remains to be tested in BCI users.

Finally, in BMI applications, one does not know a priori which area (of MI and PMv) is going to give the better decoding performance. For example, in *monkey C*, MI was typically the better area, and in *monkey G*, PMv was typically the better area. In this study, we provide an estimate of the difference in decoding performance between implanting only one array (and it being in the worse area for that kinematic parameter/monkey/session) and having two implanted arrays (Fig. 8*B*), allowing for future studies to determine the trade-off in improved decoding performance versus surgical risks/costs with dual versus single arrays. Future studies might also enable the use of noninvasive methods (e.g., functional brain imaging) to determine a priori which area might yield better performance.

ACKNOWLEDGMENTS

The authors thank Beth Travers, Allan Rydberg, and Loretta Reiss for their assistance with animal care and instrumentation design and Dr. John M. K. Mislow for surgical expertise. Part of this research was conducted using computational resources and services at the Center for Computation and Visualization, Brown University.

GRANTS

This research project was supported by the National Institutes of Health [National Institute of Neurological Disorders and Stroke (NINDS) F32-NS-061483, NS-25074, RO1-EB-007401-01] the National Center for Research Resources (NCRR C06-16549-01A1), the National Science Foundation (IIS-0534858), the Office of Naval Research (N00014-07-1-0803, award N00014-16-1-0692), NINDS Career Award 5K01-NS-057389 (W. Truccolo), DARPA (N66001-10-C-2010), the Katie Samson Foundation, Dana Foundation, Brown Brain Science Fellowship (A. K. Bansal), and the Office of Research and Development, Rehabilitation R & D Service, Department of Veterans Affairs.

DISCLOSURES

J. P. Donoghue: Prior Chief Scientific Officer and director, stock holdings, Cyberkinetics Neurotechnology Inc. (ceased operations 2009).

AUTHOR CONTRIBUTIONS

Author contributions: A.K.B., W.T., C.E.V.-I., and J.P.D. conception and design of research; A.K.B. and C.E.V.-I. performed experiments; A.K.B. and W.T. analyzed data; A.K.B., W.T., C.E.V.-I., and J.P.D. interpreted results of

experiments; A.K.B. prepared figures; A.K.B. drafted manuscript; A.K.B., W.T., C.E.V.-I., and J.P.D. edited and revised manuscript; A.K.B., W.T., C.E.V.-I., and J.P.D. approved final version of manuscript.

REFERENCES

Ajiboye A, Hochberg LR, Donoghue JP, Kirsch RF. Application of system identification methods for decoding imagined single-joint movements in an individual with high tetraplegia. *Conf Proc IEEE Eng Med Biol Soc* 2010: 2678–2681, 2010.

Artemiadis P, Shakhnarovich G, Vargas-Irwin C, Black M, Donoghue J. Decoding grasp aperture from motor-cortical population activity. *Third International IEEE EMBS Conference on Neural Engineering*, p. 518–521, 2007.

Bansal AK, Vargas-Irwin CE, Truccolo W, Donoghue JP. Relationships among low-frequency local field potentials, spiking activity, and three-dimensional reach and grasp kinematics in primary motor and ventral premotor cortices. *J Neurophysiol* 105: 1603–1619, 2011.

Belitski A, Gretton A, Magri C, Murayama Y, Montemurro MA, Logothetis NK, Panzeri S. Low-frequency local field potentials and spikes in primary visual cortex convey independent visual information. *J Neurosci* 28: 5696–5709, 2008.

Belitski A, Panzeri S, Magri C, Logothetis NK, Kayser C. Sensory information in local field potentials and spikes from visual and auditory cortices: time scales and frequency bands. *J Comput Neurosci* 29: 533–545, 2010.

Bouyer JJ, Joseph JP, Rougeul A. Effects of two neuroleptic drugs on focal somatoparietal rhythms in free awake cats. *Psychopharmacology (Berl)* 65: 55–58, 1979.

Bradberry TJ, Gentili RJ, Contreras-Vidal JL. Reconstructing three-dimensional hand movements from noninvasive electroencephalographic signals. *J Neurosci* 30: 3432–3437, 2010.

Carmena JM, Lebedev MA, Crist RE, O'Doherty JE, Santucci DM, Dimitrov DF, Patil PG, Henriquez CS, Nicolelis MA. Learning to control a brain-machine interface for reaching and grasping by primates. *PLoS Biol* 1: E42, 2003.

Chao ZC, Nagasaka Y, Fujii N. Long-term asynchronous decoding of arm motion using electrocorticographic signals in monkeys. *Front Neuroengineering* 3: 3, 2010.

Chestek CA, Cunningham JP, Gilja V, Nuyujukian P, Ryu SI, Shenoy KV. Neural prosthetic systems: current problems and future directions. *Conf Proc IEEE Eng Med Biol Soc* 2009: 3369–3375, 2009.

Craggs MD. Cortical control of motor prostheses: using the cord-transected baboon as the primate model for human paraplegia. *Adv Neurol* 10: 91–101, 1975.

Dickey AS, Suminski A, Amit Y, Hatsopoulos NG. Single-unit stability using chronically implanted multielectrode arrays. *J Neurophysiol* 102: 1331–1339, 2009.

Fetz EE. Operant conditioning of cortical unit activity. *Science* 163: 955–957, 1969.

Fluet MC, Baumann MA, Scherberger H. Context-specific grasp movement representation in macaque ventral premotor cortex. *J Neurosci* 30: 15175–15184, 2010.

Ganguly K, Carmena JM. Emergence of a stable cortical map for neuroprosthetic control. *PLoS Biol* 7: e1000153, 2009.

Graziano MS, Taylor CS, Moore T, Cooke DF. The cortical control of movement revisited. *Neuron* 36: 349–362, 2002.

Graziano MS, Aflalo TN. Rethinking cortical organization: moving away from discrete areas arranged in hierarchies. *Neuroscientist* 13: 138–147, 2007.

Hendrix CM, Mason CR, Ebner TJ. Signaling of grasp dimension and grasp force in dorsal premotor cortex and primary motor cortex neurons during reach to grasp in the monkey. *J Neurophysiol* 102: 132–145, 2009.

Hochberg LR, Serruya MD, Friehs GM, Mukand JA, Saleh M, Caplan AH, Branner A, Chen D, Penn RD, Donoghue JP. Neuronal ensemble control of prosthetic devices by a human with tetraplegia. *Nature* 442: 164–171, 2006.

Hwang EJ, Andersen RA. Brain control of movement execution onset using local field potentials in posterior parietal cortex. *J Neurosci* 29: 14363–14370, 2009.

Kaiser JF. Nonrecursive digital filter design using the -sinh window function. *Proc 1974 IEEE Symp Circuits and Systems*, p. 20–23, 1974.

Kurata K, Tanji J. Premotor cortex neurons in macaques: activity before distal and proximal forelimb movements. *J Neurosci* 6: 403–411, 1986.

Lebedev MA, O'Doherty JE, Nicolelis MA. Decoding of temporal intervals from cortical ensemble activity. *J Neurophysiol* 99: 166–186, 2008.

Lemon RN. The GL Brown Prize Lecture. Cortical control of the primate hand. *Exp Physiol* 78: 263–301, 1993.

Logothetis NK. The neural basis of the blood-oxygen-level-dependent functional magnetic resonance imaging signal. *Philos Trans R Soc Lond B Biol Sci* 357: 1003–1037, 2002.

Mehring C, Rickert J, Vaadia E, Cardosa de Oliveira S, Aertsen A, Rotter S. Inference of hand movements from local field potentials in monkey motor cortex. *Nat Neurosci* 6: 1253–1254, 2003.

Mitzdorf U. Current source-density method and application in cat cerebral cortex: investigation of evoked potentials and EEG phenomena. *Physiol Rev* 65: 37–100, 1985.

Moritz CT, Perlmutter SI, Fetz EE. Direct control of paralysed muscles by cortical neurons. *Nature* 456: 639–642, 2008.

Nicolelis MA, Lebedev MA. Principles of neural ensemble physiology underlying the operation of brain-machine interfaces. *Nat Rev Neurosci* 10: 530–540, 2009.

Nowlis DP, Kamiya J. The control of electroencephalographic alpha rhythms through auditory feedback and the associated mental activity. *Psychophysiology* 6: 476–484, 1970.

Panzeri S, Brunel N, Logothetis NK, Kayser C. Sensory neural codes using multiplexed temporal scales. *Trends Neurosci* 33: 111–120, 2010.

Pfurtscheller G, Allison BZ, Brunner C, Bauernfeind G, Solis-Escalante T, Scherer R, Zander TO, Mueller-Putz G, Neuper C, Birbaumer N. The hybrid BCI. *Front Neurosci* 4: 42, 2010.

Pistohl T, Ball T, Schulze-Bonhage A, Aertsen A, Mehring C. Prediction of arm movement trajectories from ECoG-recordings in humans. *J Neurosci Methods* 167: 105–114, 2008.

Plotkin WB. On the self-regulation of the occipital alpha rhythm: control strategies, states of consciousness, and the role of physiological feedback. *J Exp Psychol Gen* 105: 66–99, 1976.

Prabhu G, Shimazu H, Cerri G, Brochier T, Spinks RL, Maier MA, Lemon RN. Modulation of primary motor cortex outputs from ventral premotor cortex during visually guided grasp in the macaque monkey. *J Physiol* 587: 1057–1069, 2009.

Rasch MJ, Gretton A, Murayama Y, Maass W, Logothetis NK. Inferring spike trains from local field potentials. *J Neurophysiol* 99: 1461–1476, 2008.

Rickert J, Oliveira SC, Vaadia E, Aertsen A, Rotter S, Mehring C. Encoding of movement direction in different frequency ranges of motor cortical local field potentials. *J Neurosci* 25: 8815–8824, 2005.

Rizzolatti G, Camarda R, Fogassi L, Gentilucci M, Luppino G, Matelli M. Functional organization of inferior area 6 in the macaque monkey. II. Area F5 and the control of distal movements. *Exp Brain Res* 71: 491–507, 1988.

Rizzolatti G, Fogassi L, Gallese V. Motor and cognitive functions of the ventral premotor cortex. *Curr Opin Neurobiol* 12: 149–154, 2002.

Santucci DM, Kralik JD, Lebedev MA. Frontal and parietal cortical ensembles predict single-trial muscle activity during reaching movements in primates. *Eur J Neurosci* 22: 1529–1540, 2005.

Schalk G, Kubanek J, Miller KJ, Anderson NR, Leuthardt EC, Ojemann JG, Limbrick D, Moran D, Gerhardt LA, Wolpaw JR. Decoding two-dimensional movement trajectories using electrocorticographic signals in humans. *J Neural Eng* 4: 264–275, 2007.

Scherberger H, Jarvis MR, Andersen RA. Cortical local field potential encodes movement intentions in the posterior parietal cortex. *Neuron* 46: 347–354, 2005.

Stark E, Abeles M. Predicting movement from multiunit activity. *J Neurosci* 27: 8387–8394, 2007.

Stark E, Asher I, Abeles M. Encoding of reach and grasp by single neurons in premotor cortex is independent of recording site. *J Neurophysiol* 97: 3351–3364, 2007.

Suner S, Fellows MR, Vargas-Irwin C, Nakata GK, Donoghue JP. Reliability of signals from a chronically implanted, silicon-based electrode array in non-human primate primary motor cortex. *IEEE Trans Neural Syst Rehabil Eng* 13: 524–541, 2005.

Umilta MA, Brochier T, Spinks RL, Lemon RN. Simultaneous recording of macaque premotor and primary motor cortex neuronal populations reveals different functional contributions to visuomotor grasp. *J Neurophysiol* 98: 488–501, 2007.

Vargas-Irwin C, Donoghue JP. Automated spike sorting using density grid contour clustering and subtractive waveform decomposition. *J Neurosci Methods* 164: 1–18, 2007.

Vargas-Irwin CE, Shakhnarovich G, Yadollahpour P, Mislow JM, Black MJ, Donoghue JP. Decoding complete reach and grasp actions from local primary motor cortex populations. *J Neurosci* 30: 9659–9669, 2010.

Waldert S, Pistohl T, Braun C, Ball T, Aertsen A, Mehring C. A review on directional information in neural signals for brain-machine interfaces. *J Physiol (Paris)* 103: 244–254, 2009.

Waldert S, Preissl H, Demandt E, Braun C, Birbaumer N, Aertsen A, Mehring C. Hand movement direction decoded from MEG and EEG. *J Neurosci* 28: 1000–1008, 2008.

Wessberg J, Stambaugh CR, Kralik JD, Beck PD, Laubach M, Chapin JK, Kim J, Biggs SJ, Srinivasan MA, Nicolelis MA. Real-time prediction of hand trajectory by ensembles of cortical neurons in primates. *Nature* 408: 361–365, 2000.

Westwick DT, Pohlmeyer EA, Solla SA, Miller LE, Perreault EJ. Identification of multiple-input systems with highly coupled inputs: application to EMG prediction from multiple intracortical electrodes. *Neural Comput* 18: 329–355, 2006.

Wolpaw JR, McFarland DJ. Control of a two-dimensional movement signal by a noninvasive brain-computer interface in humans. *Proc Natl Acad Sci USA* 101: 17849–17854, 2004.

Wu W, Gao Y, Bienenstock E, Donoghue JP, Black MJ. Bayesian population decoding of motor cortical activity using a Kalman filter. *Neural Comput* 18: 80–118, 2006.

Xiao J, Padoa-Schioppa C, Bizzi E. Neuronal correlates of movement dynamics in the dorsal and ventral premotor area in the monkey. *Exp Brain Res* 168: 106–119, 2006.

Zhuang J, Truccolo W, Vargas-Irwin C, Donoghue JP. Decoding 3-D reach and grasp kinematics from high-frequency local field potentials in primate primary motor cortex. *IEEE Trans Biomed Eng* 57: 1774–1784, 2010.